AMPEX

ADDENDUM NO. 1 TO FINAL DEVELOPMENT REPORT

RR 68-22

27 Sept. 1968

This work was performed for the Jet Propulsion Laboratory, California Institute of Technology, sponsored by the National Aeronautics and Space Administration under Contract NAS7-100.

Ampex Corporation
Research and Advanced Technology Division

UNCLASSIFIED

ADDENDUM

No. 1

to

FINAL DEVELOPMENT REPORT

Subcontract No. 951785
Modification No. 2
Prime Contract NAS 7-100

by

H. Lienhard
J. C. Mallinson
C. Steele

Jet Propulsion Laboratory
California Institute of Technology
4800 Oak Grove Drive
Pasadena, California 91103

SUBMITTED BY J. C. Mallinson
J. C. Mallinson
Project Engineer

APPROVED BY V. E. Ragosine
V. E. Ragosine
Manager, Research Department

Ampex Corporation
401 Broadway
Redwood City, California 94063

NOTICE

This report was prepared as an account of Government sponsored work. Neither the United States, nor the National Aeronautics and Space Administration (NASA), nor any person acting on behalf of NASA:

a. Makes warranty or representation, expressed or implied, with respect to the accuracy, completeness, or usefulness of the information contained in this report, or that the use of any information, apparatus, method, or process disclosed in this report may not infringe privately-owned rights; or

b. Assumes any liabilities with respect to the use of, or for damages resulting from the use of any information, apparatus, method, or process disclosed in this report.

As used above, "person acting on behalf of NASA", includes any employee or contractor of NASA, or employee of such contractor, to the extent that such employees or contractor of NASA, or employee of such contractor prepares, disseminates, or provides access to, any information pursuant to his employment with such contractor.

Requests for copies of this report should be referred to:

National Aeronautics and Space Administration
Office of Scientific and Technical Information
Washington 25, D.C.

Attention: AFSS-A

ABSTRACT

It is proven that the linear superposition of isolated transition voltage pulses (termed "pseudo-linearity") can yield precisely the same result as the multibit computer simulation previously described.

The factors controlling the isolated pulse shape are discussed.

The impact of the "pseudo-linearity" concept upon the design of linear filters intended to alleviate the "pulse crowding" effects evident at high bit densities is analyzed.

One class of linear filters, termed "noise-whitening filters" are calculated in detail. Multibit, 7500 bpi, frequency doubling waveforms are computed with and without filtering. For high signal-to-noise ratios the filtered waveforms demonstrate that nearly all "pulse-crowding" can be removed.

Finally, the "noise-whitening" filters are reduced to simple, twelve element passive networks.

CONTENTS

1.0 INTRODUCTION

The principal purpose of this study was the undertaking of a critical review of the existing experimentally verified digital recording computer program in order to seek out both the domain of validity and reasons for the "pseudo-linearity" concept. This concept is simply that it is possible, under certain circumstances, by the linear addition of the appropriate series of isolated transition output voltage pulses, to obtain, with little error, the correct multibit voltage waveform.

Secondary objectives were: the examination of the physical factors which control the amplitude and shape of the isolated transition voltage pulse; a study, from the point of view of statistical communications theory, of the consequences of the "pseudo-linearity" concept on the over-all detection problem.

Very significant progress has been made. The reason for the "pseudo-linearity" concept is now completely understood and it has been shown to be, provided only that the record head fringing field shows a negligible rise distance (i.e. rise time multiplied by tape velocity), always applicable to "in contact" recording with standard γFe_2O_3 tape. The factors governing the isolated pulse shape are similarly almost completely understood. The effects of inter-symbol overlapping (e.g. pulse crowding) become vastly easier to comprehend when it is known that the effect arises purely by linear superposition. The possibility of using linear waveform correcting filters immediately

presents itself and it has been realized that, from the statistical point of view, the most suitable such filter is of the "noise whitening" type. This realization represents a profound advance in our understanding of the over-all detection problem and in the development of logically developed detection systems.

It has been demonstrated, by computer simulation, that realizable versions of appropriate "noise-whitening" filters do indeed effect a considerable reduction in the timing errors associated with "pulse-crowding", providing the signal-to-noise ratio is high. Specific filters have been designed for 7500 bpi, frequency doubling, 1/4 x saturation operation at four signal-to-noise ratios. Further, for each signal-to-noise ratio, four alternate twelve element passive networks have been computed which realize the required filter.

2.0 SINGLE TRANSITION VOLTAGE PULSES

2.1 Introduction

In a computer simulation of an isolated pulse it is necessary to specify four geometrical and four magnetic parameters. They are:

		Central Value Used
head-to-tape spacing	(a)	20 μin.
coating thickness	(d)	400 μin.
record gap length	(g record)	500 μin.
reproduce gap length	(g reproduce)	250 μin.
deep gap record field	(H_o)	1500 oe
range of switching fields	(H_1/H_2)	200 - 400 oe
demagnetizing permeability	μ_1	4
remagnetizing permeability	μ_2	2

One of these parameters, the head-to-tape spacing, is not known with any precision. Others are only linearized approximations. It was felt to be worthwhile to compute the output pulse as each of these parameters was varied in turn, the remainder being held constant. In addition to giving very considerable confidence that the program is functioning correctly and that no one parameter is of predominant importance, this procedure also gives a clear insight into the whole recording-demagnetizing-remagnetizing-reproducing cycle.

2.2 Theoretical Background

Before discussing the computer results, it will prove to be helpful to consider the results of three idealized calculations. The first considers the playback pulse expected from an idealized zero length transition of magnetization. According to Eldridge[1] and many subsequent authors, the output pulse is:

$$\mathcal{E}(x) \propto \log \frac{(a+d)^2 + x^2}{a^2 + x^2} \qquad (2\text{-}1)$$

If we substitute a = 20 μin, d = 400 μin, we find that the 20% to 20% pulse width would be approximately equal to 450 μin. This pulse width is much smaller than the value 1600 μin observed experimentally and the difference can only be attributed to the finite length of the magnetization transitions. This length may be due to either the original record head field gradient effect or the subsequent demagnetization process. If it is assumed that the magnetization transition has the (convenient) form;

$$M = \frac{2M_0}{\pi} \tan^{-1}\left(\frac{x}{\ell}\right) \qquad (2\text{-}2)$$

and is uniform at all depths in the tape, and that no remagnetization occurs (i.e. $\mu_2 = 1$) it may be shown[2] that the output pulse is;

$$\mathcal{E}(x) \propto \log \frac{(a+d+\ell)^2 + x^2}{(a+\ell)^2 + x^2} \qquad (2\text{-}3)$$

This expression may be made to fit the observed pulse by using $\ell \simeq 300$ μin. This corresponds to a magnetization transition shown in Fig. 1.

---

1 D. F. Eldridge, IRE Trans. Audio AU9 , 49 (1960)
2 J. J. Miyata and R. R. Hartel, IRE Trans. Elect. Comp. EC-8, 159 (1959)

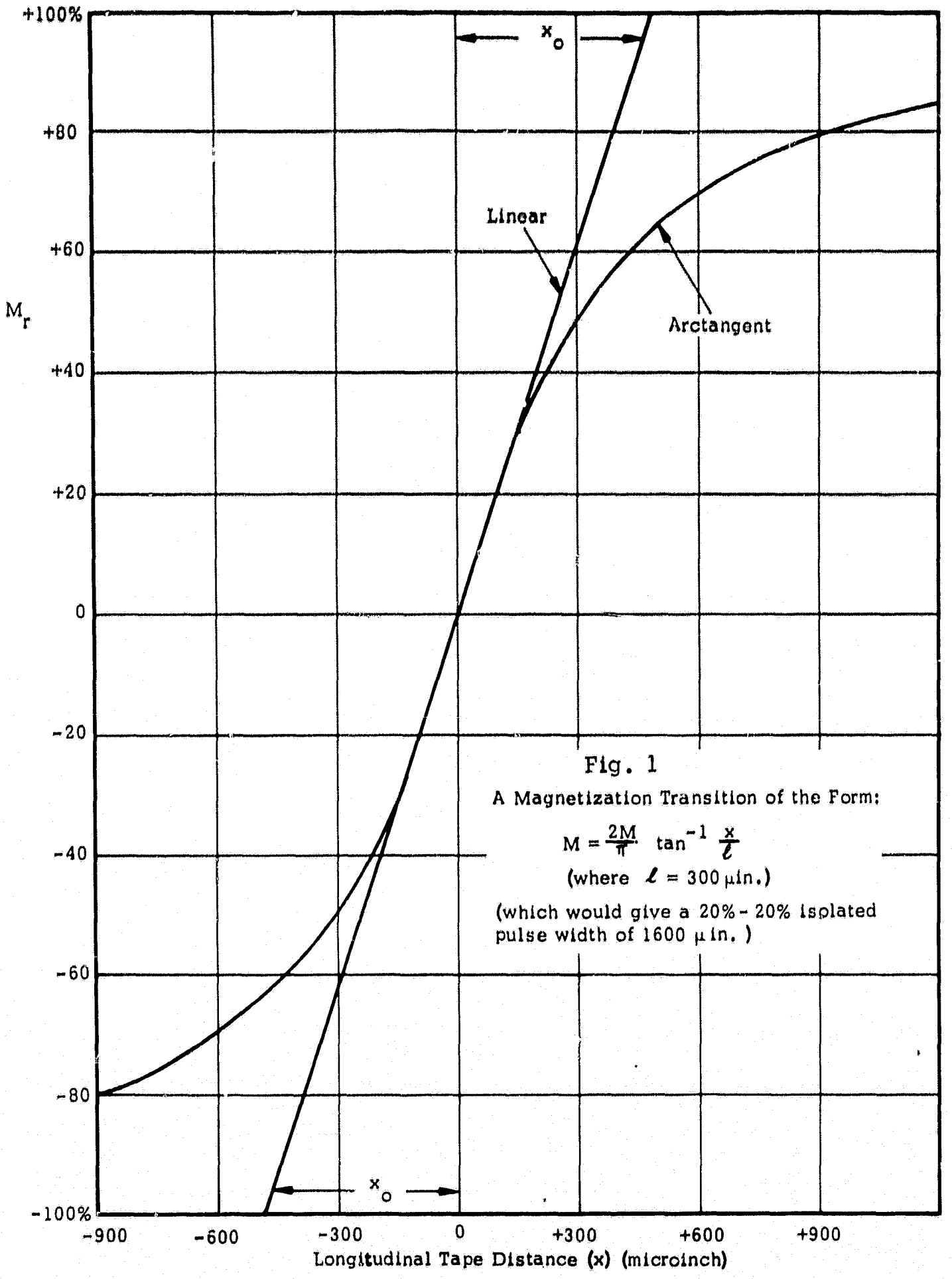

Fig. 1

A Magnetization Transition of the Form:

$$M = \frac{2M}{\pi} \tan^{-1} \frac{x}{\ell}$$

(where $\ell = 300\,\mu$in.)

(which would give a 20% - 20% isolated pulse width of 1600 μin.)

Let us now consider the linearized transition also shown (dashed line) in Fig. 1. It is drawn such that the slope at the origin coincides with that shown by the arctangent function. Th's linearized transition extends over a longitudinal distance ($2x_o$) equal to $2\,^{\pi}/_{2}$. $300 \simeq 950$ μin. We may compare this figure with that arrived at by simple estimates of the effects of demagnetization. By the somewhat ad hoc process of setting the maximum internal field equal to the coercive force of the tape coating, Speliotis and Morrison[3] give the equation;

$$\ell = 2x_o = d \cot\left(\frac{\pi}{2}\frac{H_c}{4\pi M_r}\right) \qquad (2\text{-}4)$$

For standard γFe_2O_3 tape $H_c = 300$ oe, $4\pi M_r = 1250$ gauss, yielding a transition length of approximately 900 μin, which is an excellent agreement.

We see, therefore, that, at least in the case of saturation recording on 400 μin thick γFe_2O_3, the final transition length of the magnetization is likely to be governed by demagnetization effects, to be about 900 μin long, and to give rise to a 20% - 20% output pulse width of about 1600 μin. It is, of course, difficult to separate effects but, broadly speading, about 1000 μin of the pulse width observed is due to demagnetization and about 500 μin due to the read process. Both effects can, of course, be reduced by either using thinner tape or non-saturating record currents.

2.3 Computer Results

1) Variations of the head-to-tape spacing (a)

a (μins)	ε_{peak}	Δx (μins)	20%-20% width (μins)
100	14	400	1800
60	16.5	400	1550
40	18	400	1450
20	19	400	1300
10	21	400	1150
5	22	400	1100

3 D. E. Speliotis and J.R. Morrison, IBM J. 233, May 1966

Note: Δx is the position of the reproduce pulse peak relative to the record gap centerline (i.e. it is 400 μin. downstream in this case). ε_{peak} is in relative units only.

Comments:

It is of interest, practically, that it scarcely matters whether we set the highly speculative head-to-tape spacing equal to 10 or 20 μin or even 40 μin. The variations in ε_p and 20% width thus incurred are only 15% and 25% respectively.

Theoretically, the explanation is quite simple. The transition length, ℓ, is large compared to the head-to-tape spacing, and thus;

$$\varepsilon(x) \propto \log \frac{(a+d+\ell)^2+x^2}{(a+\ell)^2+x^2} \rightarrow \log \frac{(d+\ell)^2+x^2}{\ell^2+x^2} \qquad (2\text{-}5)$$

2) Variations in coating thickness (d)

Because of the certainty of this (micrometer) measurement, this test was not made.

3) Variations in the record gap length (g record)

This test was conducted with six different gap widths and in each case the record current (deep gap field) was adjusted to give one half, once and twice the saturation level. This was determined as follows. The Karlquist arctangent head field expression may be shown to be;

$$H_x = H_0\left(\frac{\theta}{\pi}\right)$$

where θ is the angle (radians) subtended by the gap.

The maximum value of H_x occurs on the gap center line. Saturation level is defined here as being that deep gap field which just yields a field of 400 oe at the deepest tape layers, i.e.;

$$(H_o)_{sat} = 400\,\pi \Big/ 2\tan^{-1}\frac{g}{2(a+d)} \qquad (2\text{-}6)$$

H_o(oe)		ε_p	Δx	20%
2250	g record = 100 μin	15.5	200	1100
4500		19	250	1200
9000		18.5	400	1350
575	g = 500 μin	14	250	1100
1150		20	350	1200
2300		18.5	550	1350
350	g = 1000 μin	6.2	400	1300
700		19.5	600	1300
1400		19	700	1300
300	g = 1500 μin	3.8	600	1500
600		19	750	1250
1200		18.5	900	1350
--	g = 3000 μin	--	--	--
480		16.5	1400	1550
960		18	1700	1300
222	g = 5000 μin	0.5	2100	2800
445		15.5	2400	1750
890		18	2700	1400

Comments:

The principal observation is that, as is found experimentally[4], the pulse height and width at saturation are virtually independent of record gap length. This may be due to either the record field geometry or the subsequent effect of demagnetization. In Fig. 2 the record zone is drawn, to scale, for the cases of g = 100, 1000 and 3000 μin. The nesting circles are respectively the contours of constant longitudinal field strength equal to 400 and 200 oe. The shaded zone is the region of magnetization transition before any demagnetization occurs. It is quite clear that even if no demagnetization ever occurred, the output pulses derived from the g = 100 and g = 1000 μin record gaps would be virtually identical. Without demagnetization the g = 3000 μin pulse would, however, be over twice as wide. In fact, demagnetization does occur and we have already seen that it is likely to spread the transition out to almost 1000 μin. Consequently, all the pulses (g = 100, 1000 and 3000 μin) become nearly identical as the computer calculates.

4) Variations in the reproduce gap length

$g_{reproduce}$ (μins)	ε_{peak}	Δx	20% width
0	21	400	1200
250	20	400	1250
500	16.5	400	1500
750	14	400	1700
1000	11.5	400	2050

Comments:

The interesting observation here is that the case of a zero gap reproduce head, which will handle, without attenuation, even the highest harmonics, is very little better than the 250 μin. head. This may be either

4 J. J. Miyata and R. R. Hartel, IBID, Figure 14.

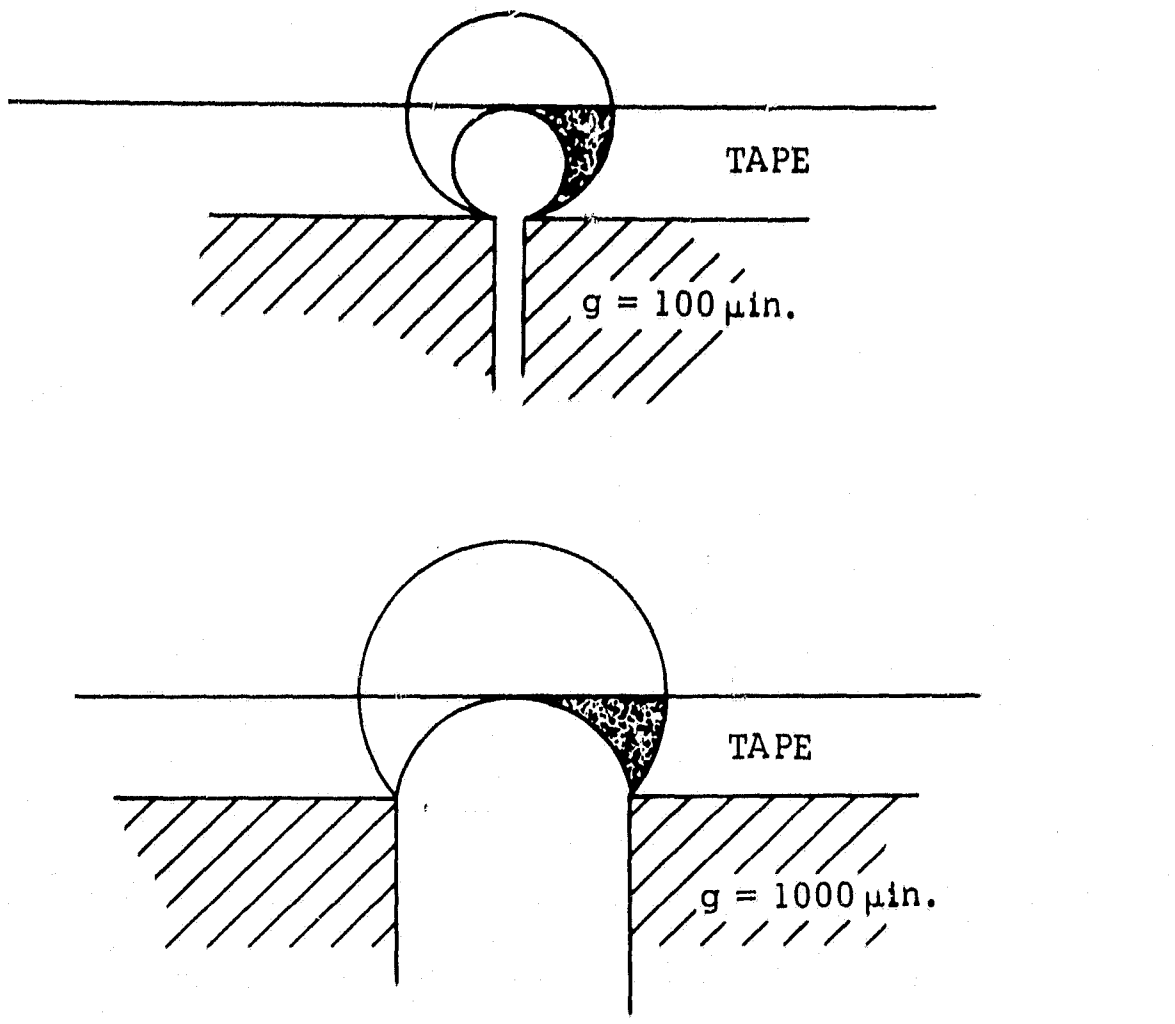

Fig. 2 Record Zones at Saturation Level

a consequence of the finite record zone length or demagnetization, either of which places an effective upper limit on the divergence of the magnetization (approx. dMx/dx in this case) and thus an upper limit on the pulse harmonics.

It would thus seem that, in practice, nothing will be gained by using reproduce gaps of length less than the coating thickness. The writer knows of no experimental data concerning this.

5) Variations in the deep gap record field (H_o)

H_o(oe)	ε_p	Δx	20% width
3000	17	600	1 400
2500	18	550	1350
2000	19	500	1300
1500	19	400	1300
1000 (sturation)	19.5	300	1200
500	14.5	200	950

Comments:

The results above are precisely as found experimentally[5]. The record zone geometries appropriate to one, two and four times saturation are drawn to scale in Fig. 3. Here we may note that, in the absence of demagnetization, the principal shortcoming of the record head field is not the much discussed "gradient" effect but rather the phase shift of longitudinal displacement of the transition zone at the various depths in the tape. Again, however, we must recall that the effects of demagnetization will effectively obliterate all the detail on a scale smaller than about 1000 μin. Consequently all the pulses above the saturation level become virtually identical.

---

5 For example, see J. J. Miyata and R. R. Hartel, IBID, Fig. 10.

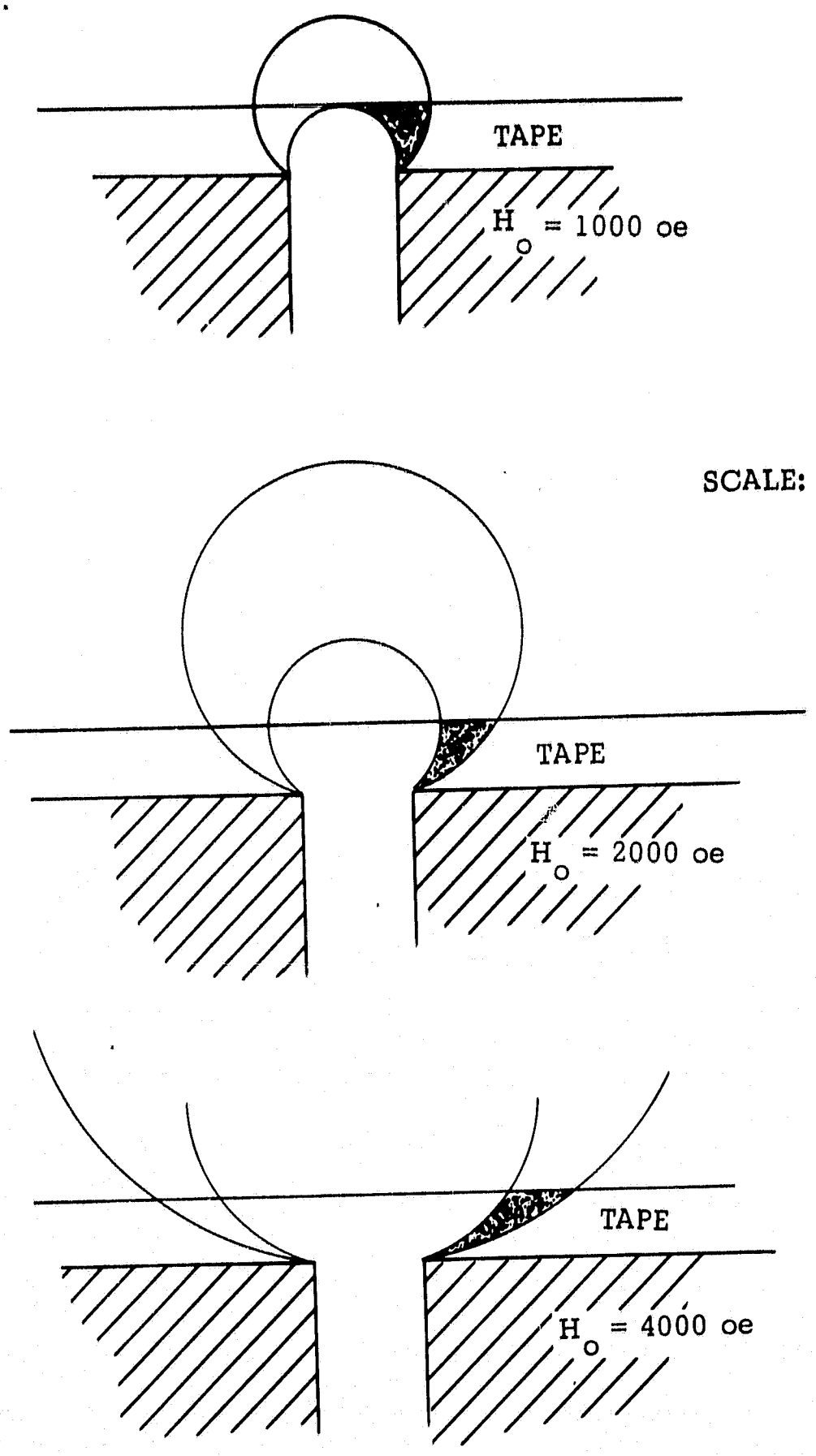

Fig. 3 Record Zones at Various Record Levels (1x, 2x and 4x saturation)

6) **Variations of the tape switching fields (H_1/H_2)**

H_1/H_2 (oe)	ε_p	Δx	20% width
200/400	19	400	1300
100/500	18	400	1400
50/550	16.5	400	1500

Note: In order that the computer program may be kept simple, all of these pairs of switching fields are made to be symmetrical about the tape coercive force, 300 oe.

Comments:

Figure 4 shows the transition zone geometry before demagnetization. Since the zone length is not large compared with the demagnetization relaxation length, very little detail survives. This case is very similar to that just considered (i.e. variation of deep gap field) and no further comment is required.

7) **Variations in the tape permeabilities (μ_1 and μ_2)**

		ε_p (g = 0)	20% width	ε_p (g = 250)	20% width
$\mu_1 = 1$	$\mu_2 = 1$	32	800	28	900
		ε_p (g = 0)	20% width	ε_p (g = 250)	20% width
$\mu_1 = 2$	$\mu_2 = 1$	24.5	900	21	1100
3		20	1100	17.5	1400
4		17	1300	15	1500
5		15	1500	13.3	1800

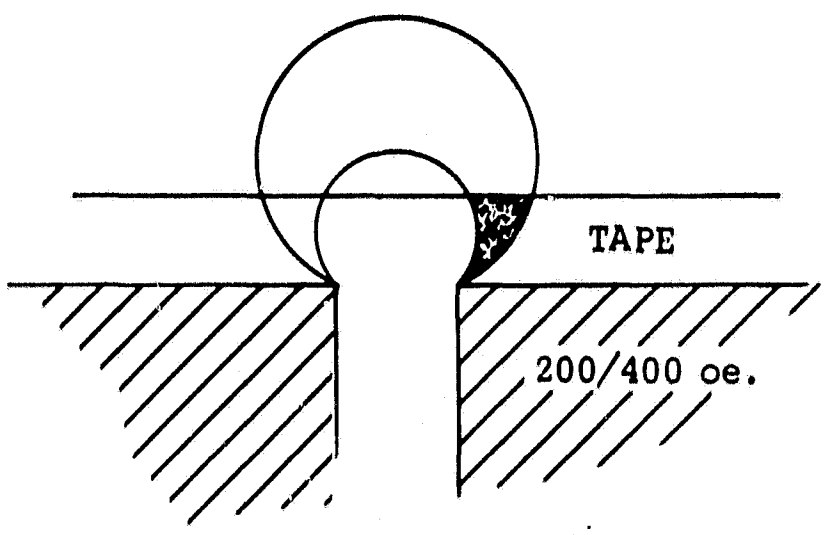

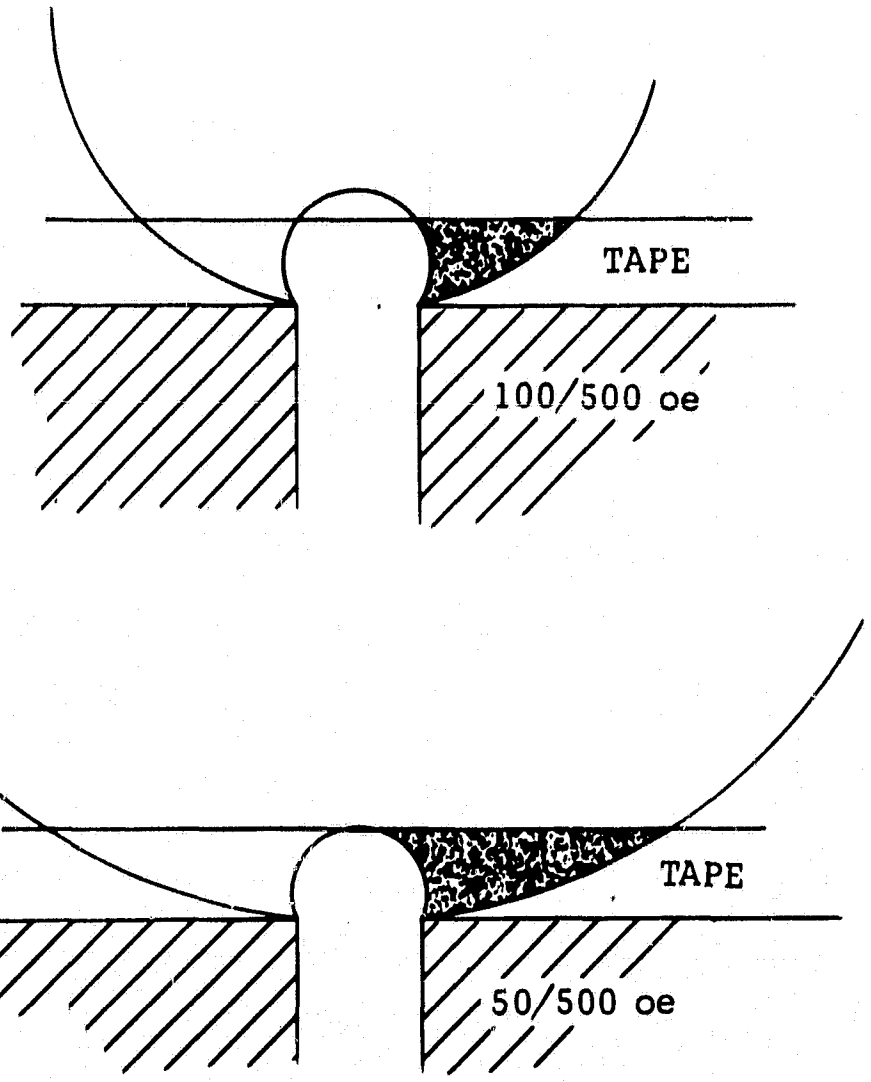

Fig. 4 Record Zones for Different Switching Fields

$\mu_1 = 2$	$\mu_2 = 2$	31	900	27	1000
3		25	1000	22.5	1200
4		21	1100	19	1300
5		18.5	1300	16.5	1400

Note: This calculation was repeated, as shown above, for the case of an ideal (g = 0) reproduce head since it is of interest to be able to separate tape and head effects.

Comments:

First, we note that the case of completely reversible demagnetization ($\mu_1 = 2$, $\mu_2 = 2$) yields virtually the same result as the case of no demagnetization ($\mu_1 = 1$, $\mu_2 = 1$). This is, of course, to be expected.

Next we notice that there is very little difference between the g = 0 and g = 250 μins. reproduce gap data. It has already been pointed out that this could be due either to record zone or demagnetization effects. It is interesting that the effect persists even for no demagnetization ($\mu_1 = 1$, $\mu_2 = 1$), and we may explain this by noting that the average record zone length is generally about 300 μin. We conclude then that even the original transition is low in harmonics of wavelength less than 300 μin.

Finally, we notice that, as anticipated, the effect of increasing μ_1 is to spread the pulse out and conversely with μ_2. It may be shown[6] that, at the short wavelength limit ($kd = 2\pi d/\lambda > 1$), the output signal becomes attenuated by a factor equal to $\mu_2 + 1/\mu_1 + 1$ if the head-to-tape spacing is negligible ($ka = 2\pi a/\lambda < 1$).

6. J. C. Mallinson, IRE Trans. Mag. 2, 3, 233, September 1966.

This condition is obeyed by wavelengths equal to the coating thickness (kd ≈ 6, ka ≈ 0.3). The attenuation factor is, for the standard case, $\mu_1 = 4$, $\mu_2 = 2$, equal to 0.6 and we may note with satisfaction that the computer yields peak voltage ratios of 21/32 = 0.66 and 19/28 = 0.68. To a good approximation then, the demag-remag cycle reduces the peak output by the factor of $\mu_2 + 1/\mu_1 + 1$.

2.4 Conclusions

1) A zero length transition would yield a 20% pulse width of about 450 μin.

2) An actual recorded transition is, before demagnetization, about 3-400 μin. long, has negligible harmonic content below λ = 3 - 400 μin. and yields a 20% pulse width of about 8 - 900 μin.

3) An actual recorded transition is, after demagnetization, about 900 - 1000 μin. long, has negligible harmonic content below λ = 3 - 400 μin, and yields a 20% pulse width of about 13 - 1400 μin.

3.0 "PSEUDO-LINEARITY"

3.1 Survey of Previously Published Work

Many authors have claimed that a multi-bit waveform can be synthesized by the linear addition of appropriate single transition output pulses. It has been generally agreed that, since all physical processes which occur after the writing process can be considered linear, linear superposition should always be found providing the transitions, as written, do not overlap. The nonlinear write mechanisms are, however, specifically excluded. Thus Hoagland and Bacon[1] state, on pages 266 and 267, "This magnetization transition width places an expected upper bound on the applicability of superposition ..... the maximum bit density that can be anticipated as susceptible to superposition simulation is 2500 bpi." The bit density refers to NRZ, in the Frequency Doubling context the limit would be 1250 bpi (2500 frpi).

More recent engineering studies[2,3] have invariably assumed "pseudo-linearity", but have not stated any specific limitations. Morrison and Speliotis[4] report, in an experimental paper, that linear superposition was applicable up to 60,000 frpi; this statement was applied, however, to the cases of thin metallic media where the coating thicknesses are of the order tens of microinches. It seems likely

---

1 A.S.Hoagland and G.C.Bacon, Proc. IRE 49, pp 258-267, Jan.1961
2 W.W.Chu, IRE Trans.,Elect. Computers, EC-15, 3 pp 328-336, June 1966
3 H.M.Sierra,Electro-Technology, 78, 3 pp 56-58, Sept. 1966
4 J.R.Morrison and D.E.Speliotis, IEEE Trans, MAG MAG-3, 3, pp 308-311, September 1967

in these cases, that the length of written magnetization transition will be of the same order of magnitude and that, consequently Hoagland and Bacon's criterion still holds. Finally, in the Final Development Report, presented in December 1967, the regions of expected applicability of "pseudo-linearity" were clearly delineated. (see Figs. 10-13, pp 39-42, title "Pulse Crowding Data", Final Development Report, Ampex No. RR67-36.)

3.2 A Proof That "Pseudo-Linearity" is an Intrinsic Part of the Present Computer Simulation Algorithm

It is required to prove that if one adds together the appropriate series of isolated output voltage pulses, the result is identical with the multi-bit output voltage waveform as computed in our present program (e.g. JPL 4).

In order to demonstrate this property of pseudo-linearity, it is sufficient to consider the record head field history and initial remanent magnetization (abbreviated to initial magnetization) acquired by an arbitrary point in the tape as it passes the record head.

In this proof, we shall first show that a linear superposition of the initial magnetization patterns which result from the application of isolated step transitions of record current gives, except for a possible x (longitudinal coordinate) invariant term, precisely the multi-bit initial magnetization waveform.

We first consider the multi-bit case, where there occur successive field extrema, of decreasing magnitude and of alternating polarity, labeled H_1, H_2, H_3 and H_4 in Fig. 5A . These field extrema cause additive changes in the initial magnetization at that point in the tape shown, symbolically, as

½ ΔM_1, ΔM_2, ΔM_3 and ΔM_4 in Fig. 5B Note that the both the magnitude and polarity of the change in magnetization is indicated by the symbols used. The initial magnetization acquired by this point is given by:

$$M = \tfrac{1}{2}\,\Delta M_1 + \sum_{n=2}^{4} \Delta M_n \qquad (3\text{-}1)$$

It is of crucial importance to note that, according to any non-interacting loop model, each of these changes in magnetization is dependent only upon the field extremum causing that change. In our present computer program we have;

$$\Delta M_n = 0 \qquad \text{for} \quad H_n < |H_{min}| \qquad (3\text{-}2)$$

$$\Delta M_n = \chi \left[|H_n| - H_{min} \right] \frac{H_n}{|H_n|} \qquad \text{for} \quad H_{min} < |H_n| < H_{max.} \qquad (3\text{-}3)$$

$$\Delta M_n = \chi \left[H_{max} - H_{min} \right] \frac{H_n}{|H_n|} \qquad \text{for} \quad |H_n| > H_{max.} \qquad (3\text{-}4)$$

Now, turning to the single transition cases, we see that, for each such transition to be added, there exists a field diagram similar to that shown in Fig.5C. In each diagram there will be only two field extrema of significance. They are the absolute maximum field (which in our model of the head field occurs on head center line but is not, in fact, so restricted) and the reverse field extremum at the transition time. The first transition field history shown in Fig. 5C gives rise to the changes in magnetization shown, symbolically, in Fig. 5D. Note that, if the record head current is the same as was used in the multi-bit case above, the magnitude and polarity of these two changes in magnetization, ½ ΔM_1 and ΔM_2, are

identical to those shown for the multi-bit case in Fig. 5B. This occurs for the simple reason that the field histories are the same. The second transition would cause the changes in magnetization $\frac{1}{2}\Delta M_1$ and ΔM_3 shown in Fig. 5E. Although the first change is of the correct magnitude but of incorrect polarity, the change ΔM_3 is exactly as shown in the multi-bit case Fig. 5B. The third transition yields, as shown in Fig. 5F, both changes in magnetization correctly.

If all these separate transition changes in magnetization (Figs. 5D, 5E and 5F) be summed (see Fig. 5G), it is clear that exactly the correct multi-bit sequence shown in Fig. 5B results. Thus the initial magnetization which would be calculated for this point in the tape is exactly the same for both the multi-bit process and the pseudo-linearity add-up process.

It will be seen, however, that if the number of transitions to be summed be even, then a discrepancy occurs with regard to the center line transitions $\frac{1}{2}\Delta M_1$, which then sum to zero. This discrepancy is just the x invariant term mentioned above. It is x invariant because all points in the tape, at a particular depth y, experience exactly the same magnitude of field as they cross the gap center line. Apparently each depth in the tape may suffer (if the number of transitions summed be even) a different x invariant error.

To obtain the reproduce head output voltage from the initial remanent magnetization three operations are needed;

averaging through the tape depth,

demagnetization, remagnetization and flux collection,

differentiation with respect to time or tape displacement.

The averaging and differentiation operations are linear and the demag-remag-flux collection algorithm used here is also linear. As a result one

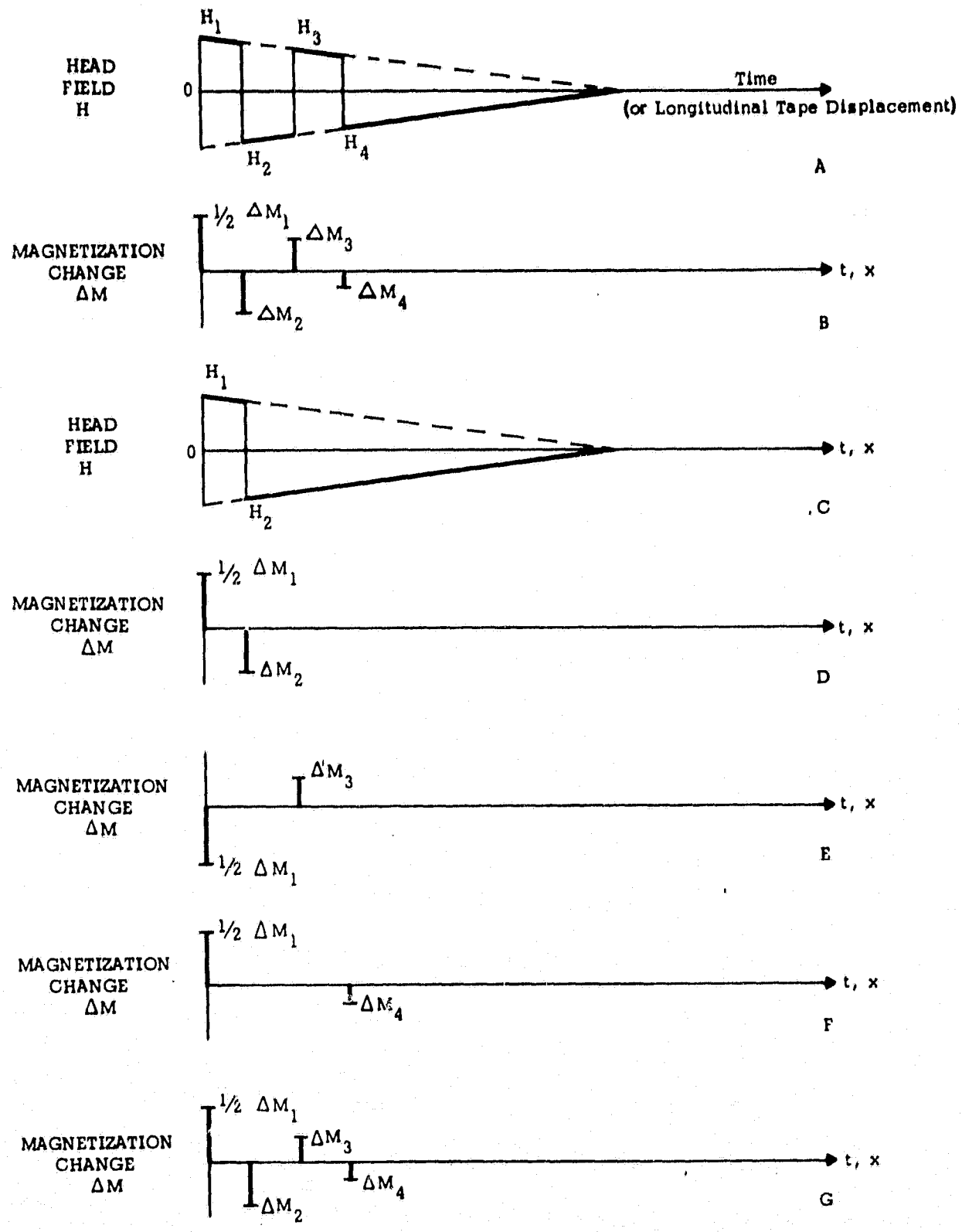

Fig. 5 Record Head Field Histories and Initial Remanent Magnetization Changes Suffered by a Point in the Tape for Both Single Transition and Multi-Transition Input Currents.

can express the output voltage as a linear operation on the derivative of the initial magnetization with respect to the longitudinal coordinate x. Since the multi-bit recorded magnetization can differ by only a constant from the sum of the corresponding single-bit recorded magnetizations, the derivative of the multi-bit magnetization with x must equal the sum of the derivatives of the single-bit magnetizations. Since the transformation from this derivative to output voltage is linear, the sum of the single-bit output voltages computed individually from the single-bit derivatives must equal the voltage that would be computed from the sum of these derivatives.

3.3 A Demonstration of the "Pseudo-Linearity" Concept

In the following figures (6-10) are shown both the directly computed waveforms and those obtained by application of the "pseudo-linearity" concept. The latter are labeled "ADD-UP". The parameters used in the calculations are:

head-to-tape spacing	(a)	20 μin.
coating thickness	(d)	400 μin.
record gap length		150 μin.
reproduce gap length		25 μin.
deep gap field	(H_o)	4500 oe (1 x sat.)
tape switching fields	H_1/H_2	100/500 oe
tape permeabilities	μ_1/μ_2	5/2

An eight bit frequency doubling word 01010011 is used and the curves have been computed for 625, 1250, 2500, 5000, and 10,000 bpi (frequency doubling). "Pseudo-linearity" is seen to hold in all cases. It was previously expected (see para. 3.1 above) to fail at about 2500 bpi. The basic reason for the applicability of "pseudo-linearity" being now

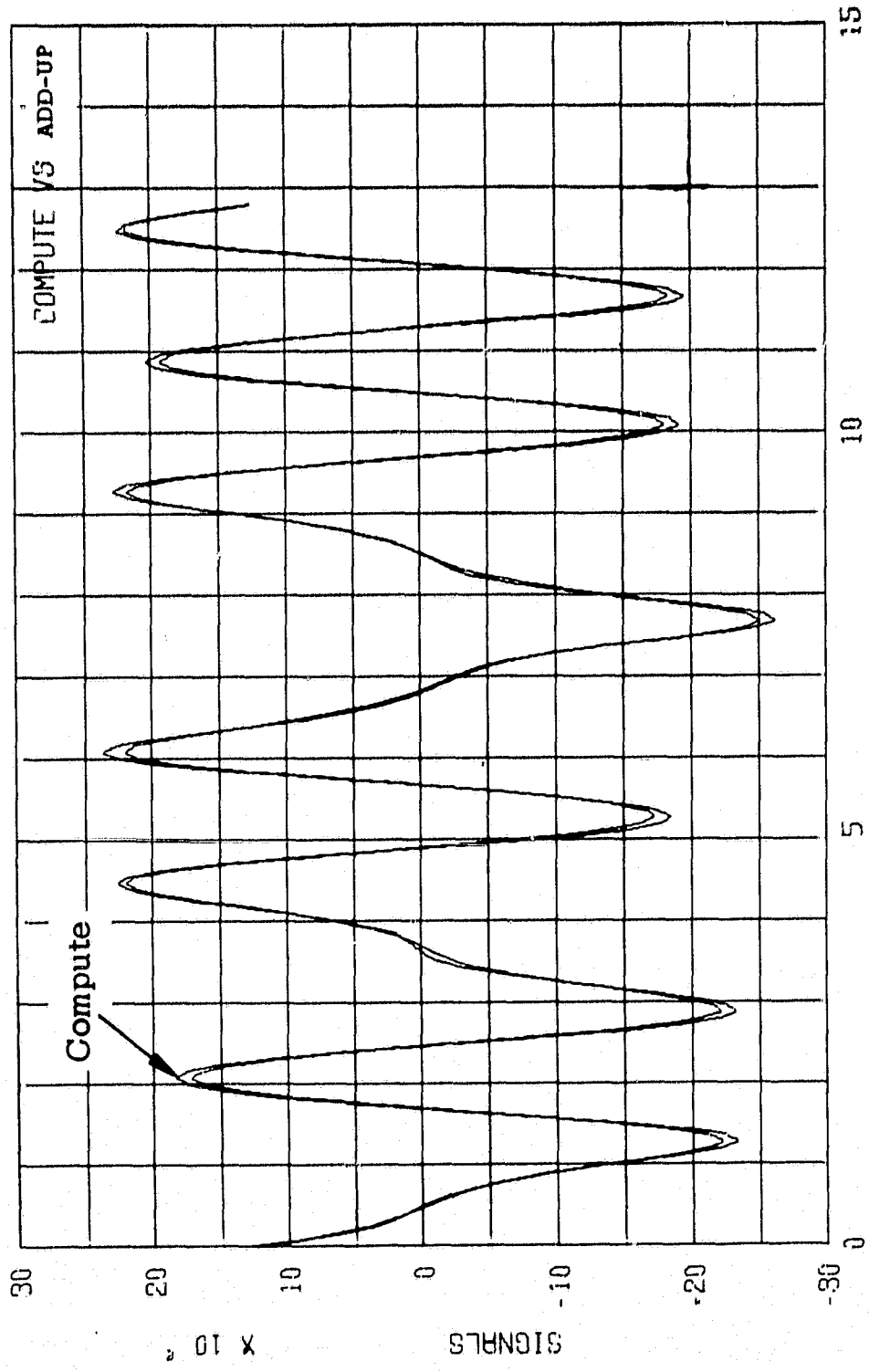

Fig. 6 Computed Multi-Bit and Single Pulse "ADD-UP" Waveforms at 625 bpi

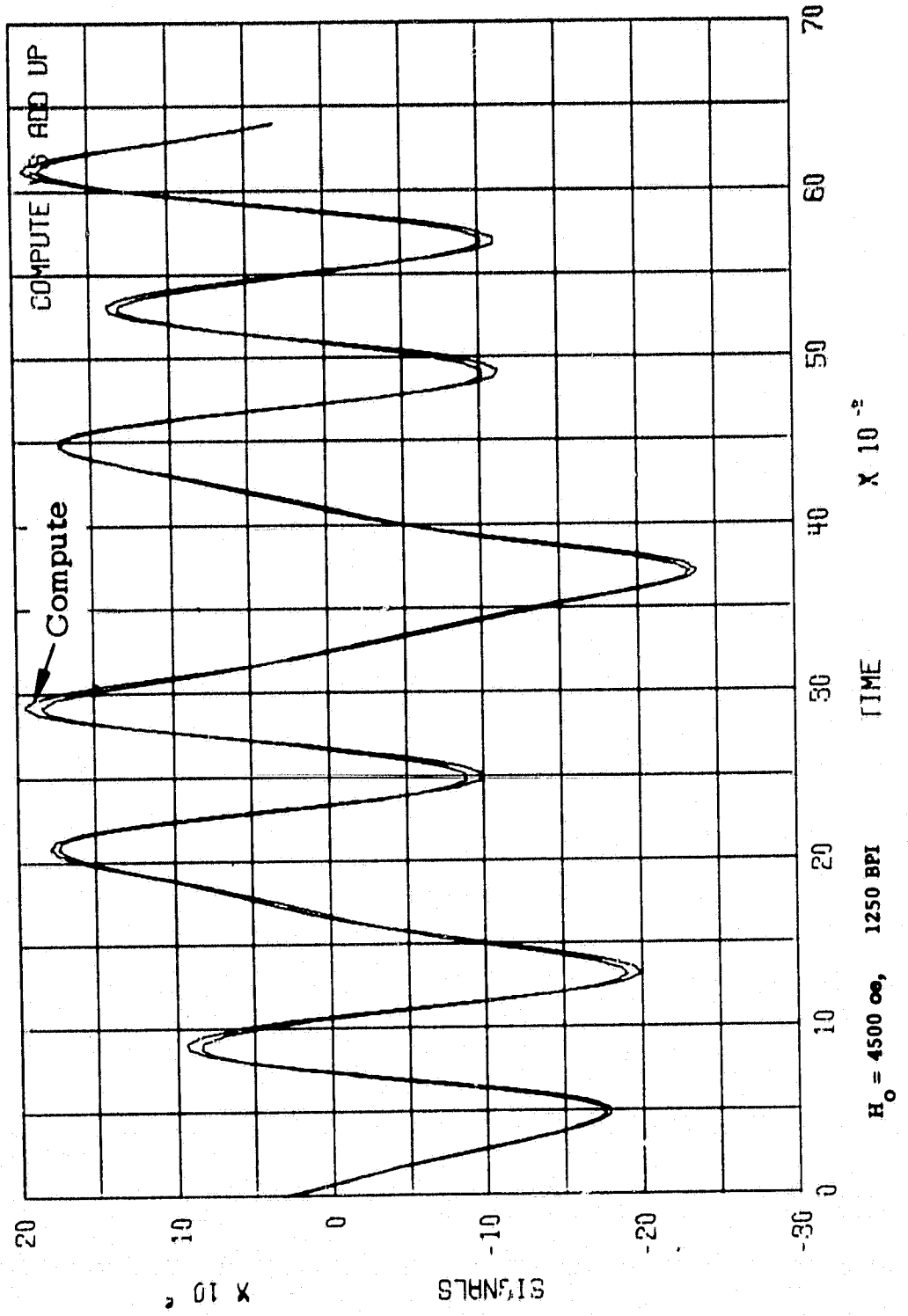

Fig. 7 Computed Multi-Bit and Single Pulse "ADD-UP" Waveforms at 1250 bpi

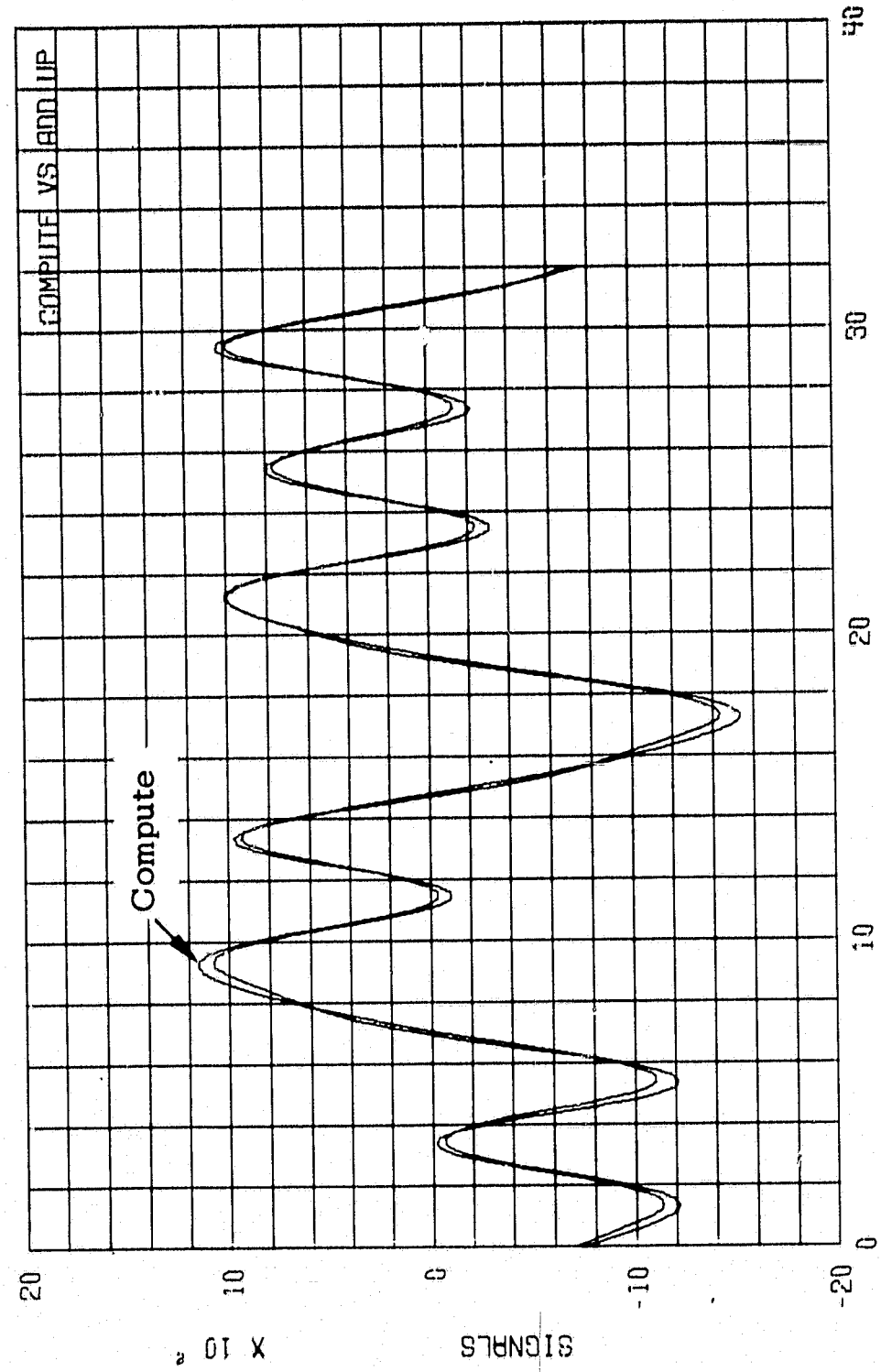

Fig. 8 Computed Multi-Bit and Single Pulse "ADD-UP" Waveforms at 2500 bpi

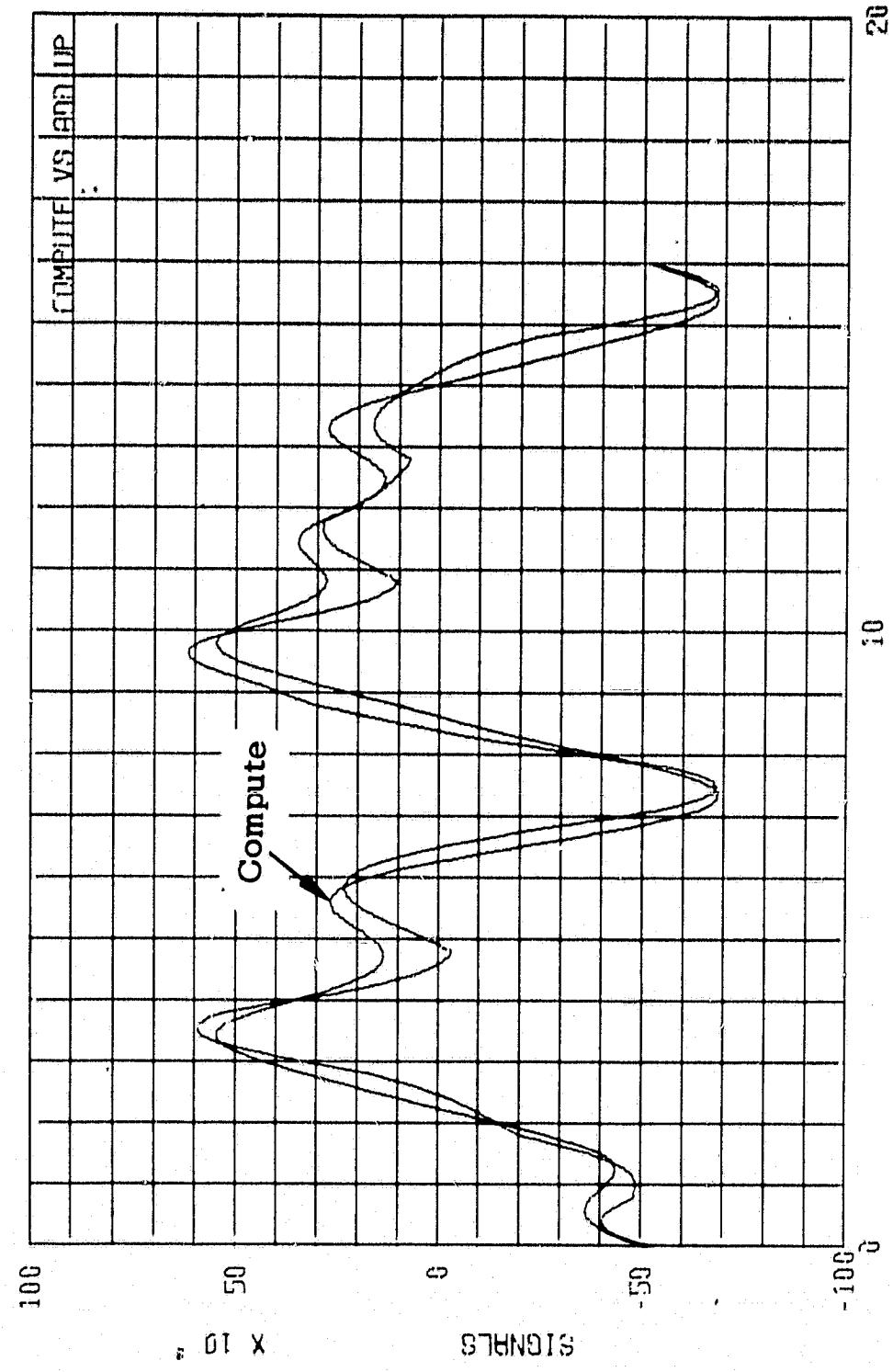

Fig. 9 Computed Multi-Bit and Single Pulse "ADD-UP" Waveforms at 5000 bpi

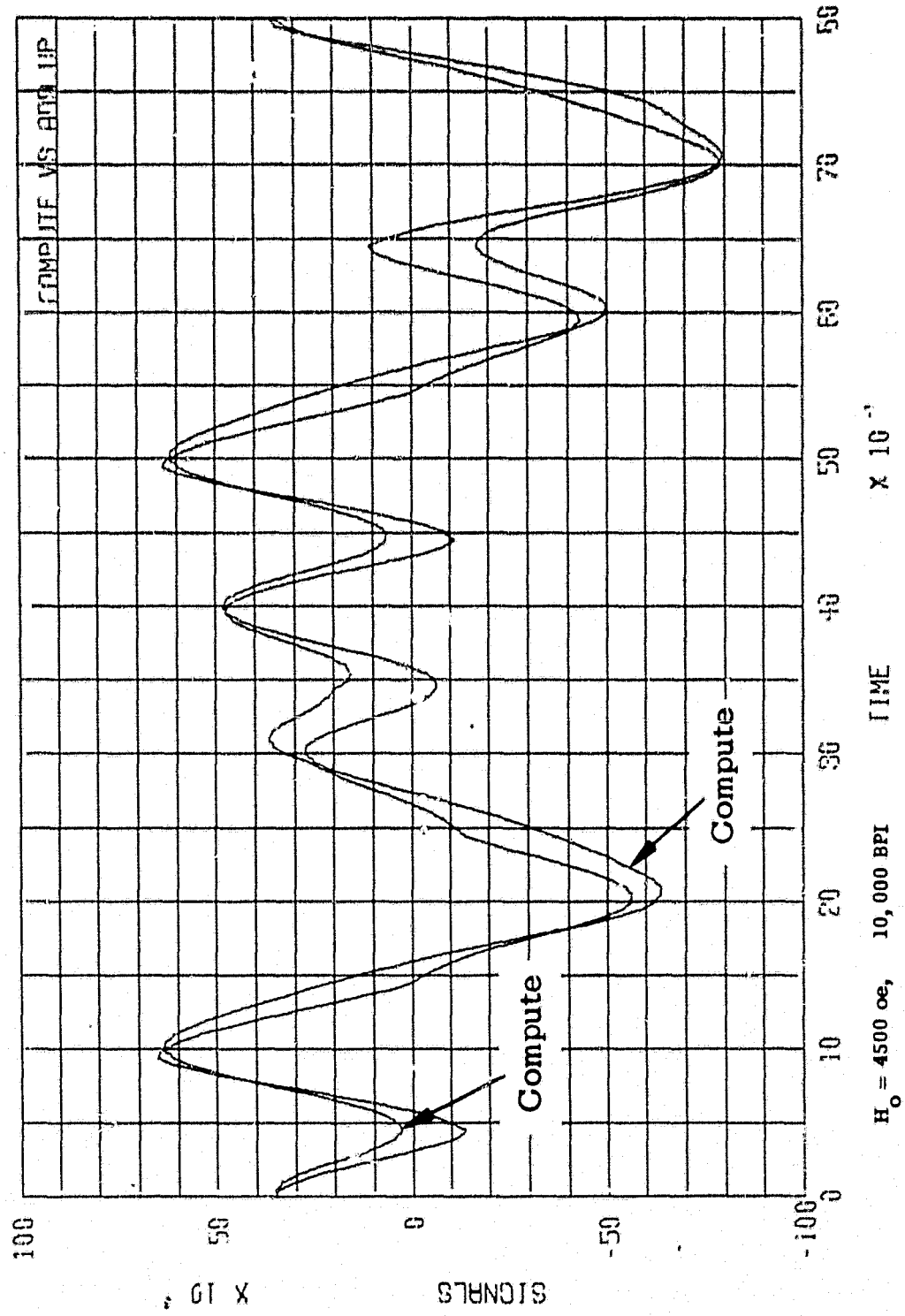

Fig. 10 Computed Multi-Bit and Single Pulse "ADD-UP" Waveforms at 10,000 bpi

fully understood, it is realized, that the slight discrepancies which occur in the computed curves are due only to computational errors. Specifically, the error occurs because the eight-bit word length becomes at the higher bit densities smaller than the single pulse length. In the preset ADD-UP program this problem has been handled by simply truncating the single pulse and, consequently, an increasing error becomes evident with increasing bit density.

3.4 Some More General Considerations of "Pseudo-Linearity"

It will have been noticed that there exist two crucial points in the proof given above that "pseudo-linearity" is intrinsic to our present computer simulation of digital recording. They are that the record head field transitions be perfect step functions (i.e. occupy zero time or tape length) and that a non-interacting $M_r - H$ model be used. Obviously neither condition can be realized physically and apparently some relaxation must be possible before the linear superposition process becomes invalid.

With regard to the rise time (or rise distance) of the head field it is clear that, since the recorder cannot reproduce wavelengths less than the reproduce head gap length, it is sufficient that the rise distance be less than the reproduce gap length. Further, since a signal of wavelength comparable to the head-to-tape spacing is attenuated by at least a factor of 500 it is sufficient that the rise distance be less than the head-to-tape spacing. In practical terms this means that the field rise distance must be less than the greater of 20 microinches or the reproduce gap length of "pseudo-linearity" to occur. Thereader is cautioned that the important factor here is the field and not the record current rise distance. Due to eddy currents and other losses the field rise distance may greatly exceed that of the record current.

The non-interacting $M_r - H$ model we have assumed throughout this study may, purely as a matter of convenience, be redrawn as a Priesach diagram (see Fig. 11). Here the assumed uniform distribution of tape switching fields (H_s) and the absence of interparticle interaction fields (H_i) lead to the Priesach function shown. It is a narrow parallelopiped standing up out of the plane of the paper (the H_i, H_s plane). The application of positive and negative fields H_1 and H_2 causes the Priesach function to be divided in corresponding positive and negative zones (whose volumes correspond to the changes of magnetization $\frac{1}{2}\Delta M_1$ and ΔM_2 discussed previously). The algebraic sum of these regions is the remanence (M_r). Note that, providing the intersection point P of the lines defining the switched regions falls outside the Priesach function, then each change in magnetization is independent of the other changes. This independence, which is a necessary condition for "pseudo-linearity", is always obtained, of course, for non-interacting Priesach functions since they are zero width. During the recording process, the position of these intersection points depends upon a variety of factors such as the bit density, the bit pattern being recorded and the head field gradient ($\partial H_x / \partial x$). In the important surface layers of the tape this field gradient is, of course, very high and the intersection points will fall well away from the $H_i = 0$ axis for all reasonable bit densities* (see Fig. 12). Consequently "pseudo-linearity" could still occur should real Priesach functions of finite width be employed in the simulation. It may be noted finally that the assumed uniformity of the distribution of particle switching fields, which property gives the $M_r - H$ loops their straight sides, plays no role in the occurrence of "pseudo-linearity".

*This fact, which in turn causes the recorded magnetization in the surface layers of the tape to be a rather insensitive function of the specific Priesach function, is undoubtedly principally responsible for the excellent agreement between theory and experiment we obtain at the high (5000-10,000 bpi) bit densities.

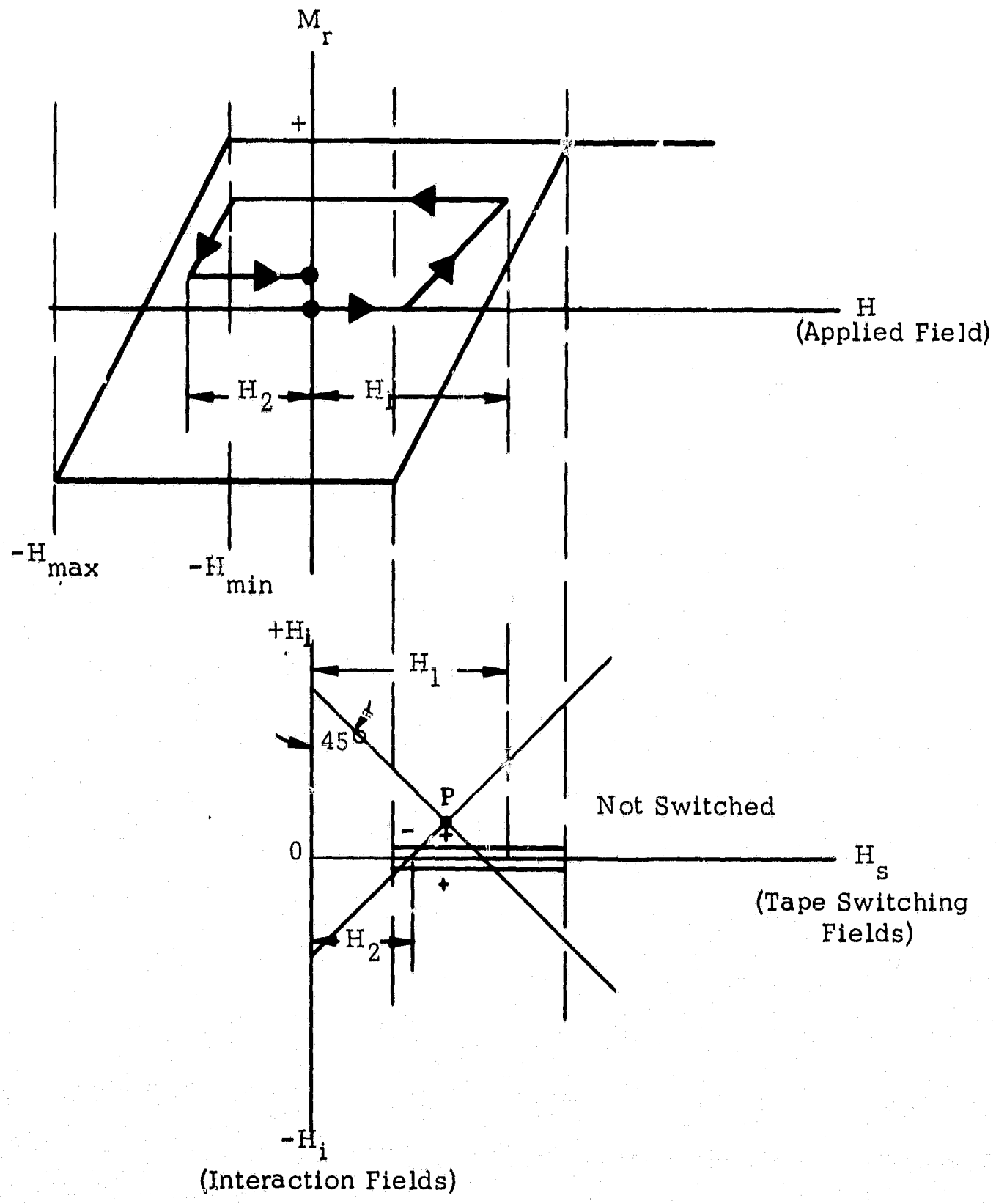

Fig. 11 The Non-Interacting M_r - H Loop and its Corresponding Preisach Diagram

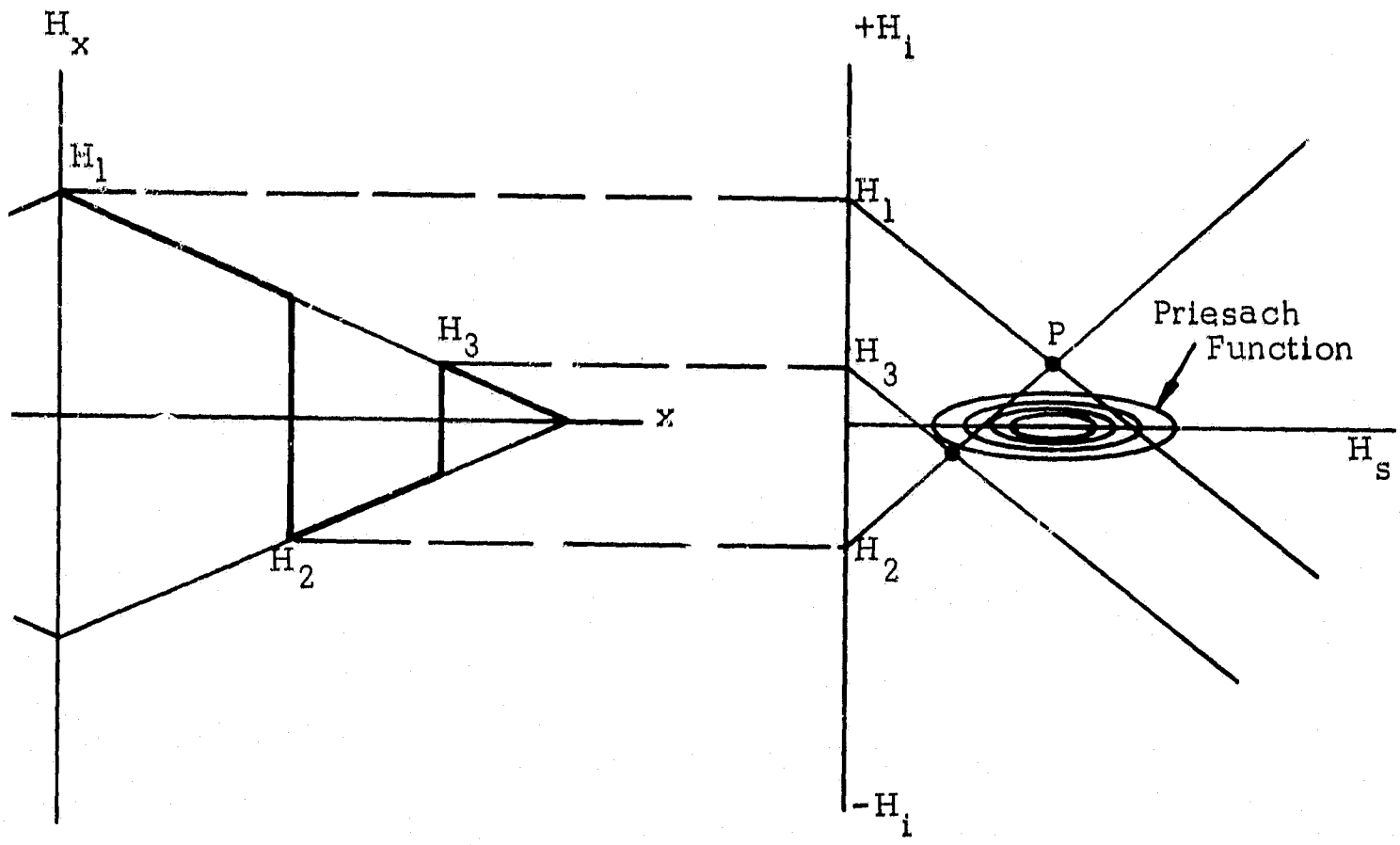

A) Head Field vs. Distance

B) Priesach Plane Representation

Fig. 12 Showing how the record head field extrema project into the Priesach plane and how the intersections (P) may fall outside the Priesach Function.

PRECEDING PAGE BLANK NOT FILMED.

4.0 THE "NOISE-WHITENING" FILTER

4.1 The "Pre-Whitening" Filter Derivation

Let $\{a_k,\ k = 0, \pm 1, \pm 2, \ldots\}$ be a sequence of independent binary-valued random variables. Each a_k having the possible values of ± 1 with equal probabilities. Suppose the output of a tape digital recorder is represented by

$$x(t) = \sum_{k=-\infty}^{\infty} a_k\, h(t - k\Delta) + n(t) \qquad (4\text{-}1)$$

To recover each a_k, we observe $x(t)$ over the interval

$$k\Delta - \tfrac{1}{2}\Delta \leq t \leq \tfrac{k}{\Delta} + \tfrac{1}{2}\Delta \quad (\Delta \text{ is the bit length})$$

and decide between the two alternative hypotheses: $a_k = 1$ and $a_k = -1$. If the noise $n(t)$ is a stationary process, then the problem is the same for each k. Therefore, our basic problem is the following: Given the observation

$$x(t) = a_0 h(t) + \sum_{k=1}^{\infty} a_k h(t - k\Delta) + \sum_{-\infty}^{-1} a_k h(t - k\Delta) + n(t) \qquad (4\text{-}2)$$

$$-\frac{\Delta}{2} \leq t \leq \frac{\Delta}{2}$$

decide whether a_0 is $+1$ or -1.

The two sums in (12) clearly represent intersymbol interference. If these two terms were absent, and if the noise n(t) is a Gaussian white noise, then the optimum detector takes on the well known form of a matched filter matched to the waveform h(t) followed by sampling and comparison On the other hand if the noise terms were absent in Eq.(4-2) then perfect detection would result from a pulse compression filter which reduces the pulse width to Δ or less, because then the two sums in (4-2) would be zero over the interval $-\Delta/2 \leq t \leq \Delta/2$. These two situations represent limiting cases at the two extremes. The detector circuit for the general situation falls somewhere in between. Our objective is to derive the form of the detector for the general case.

As far as the detection problem is concerned the effect of pulse interference is not essentially different from that of noise. We can rewrite Eq. (12) as

$$x(t) = a_0 h(t) + n'(t) \quad , -\frac{\Delta}{2} \leq t \leq \frac{\Delta}{2} \tag{4-3}$$

with $$n'(t) = n(t) + \sum_{k \neq 0} a_k h(t - k\Delta) \tag{4-4}$$

The statistical properties of the effective noise n'(t) depend not only on n(t) but also on the pulse shape h(t) and the statistical properties of the sequence $\{a_k\}$. Suppose n(t) is a white noise with zero mean and

$$E\, n(t)\, n(s) = N_0 \delta(t-s) \tag{4-5}$$

That is, the two-sided power spectral density of n(t) is N_0 (watts/cps) for all frequencies. We have already assumed that $\{a_k\}$ is a sequence

of independent random variables, each being ± 1 with equal probabilities. It is also reasonable to assume that $n(t)$ and $\{a_k\}$ are mutually independent. It follows from these assumptions that

$$E\, n'(t) = 0$$

$$E\, n'(t)\, n'(s) = N_0 \delta(t-s) + \sum_{k\neq 0} h(t-k\Delta)\, h(s-k\Delta)\, E\, a_k^2$$

$$= N_0 \delta(t-s) + \sum_{k\neq 0} h(t-k\Delta)\, h(s-k\Delta) \qquad (4\text{-}6)$$

If Δ is small, so that $h(t+\Delta) \cong h(t)$ for all t, then the sum in Eq. (4-6) can be approximated by an integral, viz.,

$$\sum_{\substack{k\neq 0 \\ k=-\infty}}^{\infty} h(t-k\Delta)\, h(s-k\Delta) = \frac{1}{\Delta} \sum_{k\neq 0} \Delta\, h(t-k\Delta)\, h(s-k\Delta)$$

$$\cong \frac{1}{\Delta} \int_{-\infty}^{\infty} h(t-\tau)\, h(s-\tau)\, d\tau \qquad (4\text{-}7)$$

$$= \frac{1}{\Delta} \int_{-\infty}^{\infty} h(t-s+\sigma)\, h(\sigma)\, d\sigma$$

The last term in Eq. (4-7) depends only on $t-s$, which shows that $n'(t)$ is approximately widesense stationary with

$$E\, n'(t)\, n'(s) \cong R(t-s) = N_0 \delta(t-s) + \frac{1}{\Delta} \int_{-\infty}^{\infty} h(t-s+\sigma)\, h(\sigma)\, d\sigma \qquad (4\text{-}8)$$

and a power spectral density function given by,

$$\phi(\omega) = \int_{-\infty}^{\infty} R(\tau)\, e^{-i\omega\tau}\, d\tau$$

$$= N_0 + \frac{1}{\Delta}\left| H(\omega)\right|^2 \qquad (4\text{-}9)$$

where $H(\omega)$ is the Fourier transform of the pulse shape $h(t)$, i.e.

$$H(\omega) = \int_{-\infty}^{\infty} h(t)\, e^{-i\omega t}\, dt \qquad (4\text{-}10)$$

The preceding analysis shows that when Δ is small in comparison with the pulse width, i.e., under conditions of severe pulse overlapping, the effect of interpulse interference is equivalent to one of changing the white noise $n(t)$ to a non-white noise $n'(t)$ with spectral density given by Eq.(4-9). But we know that a non-white noise can be whitened. Specifically, let $G(\omega)$ be the transfer function of a filter, and let $G(\omega)$ satisfy

$$\left| G(\omega)\right| = \frac{1}{\sqrt{1 + \frac{1}{N_0\Delta}\left| H(\omega)\right|^2}} \qquad (4\text{-}11)$$

If the pulse train $x(t)$ is passed through this filter, then the output will be given by

$$x_1(t) = a_0 h_1(t) + n_1(t) \qquad (4\text{-}12)$$

where $n_1(t)$ is again a white noise with spectral density equal to N_o and $h_1(t)$ is given by,

$$h_1(t) = \frac{1}{2\pi}\int_{-\infty}^{\infty} G(\omega)\, H(\omega)\, e^{i\omega t}\, d\omega$$

$$= \int_{-\infty}^{\infty} g(t-\tau)\, h(\tau)\, d\tau \qquad (4\text{-}13)$$

The effect of this prewhitening filter $G(\omega)$ is to convert the problem of detecting a pulse $a_o h(t)$ in the presence of both white noise and inter-pulse interference into one of detecting a pulse $a_o h_1(t)$ in the presence of white noise only. For large signal-noise ratio we have, for small values of ω, $|G(\omega)| \sim \frac{1}{|H(\omega)|}$ which has precisely the effect of a pulse-compression filter.

If one can assume that the white noise $n_1(t)$ is Gaussian, then the over-all optimum detector structure is completely known. It consists of the prewhitening filter $G(\omega)$ followed by a matched filter matched to the waveshape $h_1(t)$. The output of the match filter is then sampled and the sample is compared to zero. The decision is $a_o = 1$ if the sampled output is positive and $a_o = -1$ otherwise. It is important, therefore, to investigate conditions under which the white noise $n_1(t)$ is Gaussian. Unfortunately, under the assumption that we have made or under the actual conditions that are likely to occur, the noise $n_1(t)$ cannot be strictly Gaussian. However, it will be approximately Gaussian if $n(t)$ is Gaussian (which is reasonable) and if the sum $\sum_k a_k h(t - k\Delta)$ converges slowly for each t. In other words, the pulse $h(t)$ is wide compared to the bit-interval Δ. Again, this corresponds to severe pulse-overlapping or high density situation.

In summary, we have shown that the pulse-compression filter for alleviating pulse-overlapping in high-density digital recording can be interpreted as a prewhitening filter when the problem is formulated as a detection problem in the presence of both white noise and inter-symbol interference. This prewhitening filter also elucidates the behavior of the pulse-compression filter at high frequencies. The high-frequency behavior, as is expected, is noise limited. Under high-density recording conditions near-optimum detection is achieved by a sequence of operations consisting of prewhitening, matched filter, sampling, and comparison with zero, in that order.

4.2 The Computation of Realizable Noise-Whitening Filter Transfer Functions

Suitable filter transfer functions $G(\omega)$ have been found in the form

$$G(s) = \frac{(s-z_1)(s-z_2)}{(s-p_1)(s-p_2)} \qquad (4\text{-}14)$$

where z_1 and z_2 are its S-plane zeros, p_1 and p_2 are its S-plane poles and

$$s = j\omega \qquad (4\text{-}15)$$

To do this, the Fourier transform $H(\omega)$ of the output pulse shape h(t) (which corresponds to a single digital input transition) was approximated by $|H_a(\omega)|^2$ given by

$$|H_a(\omega)|^2 = \frac{|H(0)|^2}{1 + b\omega^2 + c\omega^4} \qquad (4\text{-}16)$$

by appropriate choice of the real constants b and c *. From Eq. (4-11) in paragraph 4.1 above, we have;

$$|G(\omega)|^2 = \frac{1}{1 + \frac{1}{N_0\Delta}|H_a(\omega)|^2} \qquad (4\text{-}17)$$

where Δ is the bit length and N_o is the noise spectral power density. Combining (4-16) and (4-17) yields

*See Appendices A and B.

$$|G(\omega)|^2 = \frac{1 + b\omega^2 + c\omega^4}{1 + \frac{|H(0)|^2}{N_0 \Delta} + b\omega^2 + c\omega^4} \qquad (4\text{-}18)$$

and this combined with (4-15) gives

$$|G(s)|^2 = \frac{1 - bs^2 + cs^4}{1 + \frac{|H(0)|^2}{N_0 \Delta} - bs^2 + cs^4} = \frac{P(s^2)}{Q(s^2)} \qquad (4\text{-}19)$$

G(s) in the form given in (4-14), is obtained by factorizing the numerator and denominator polynomials of s in (4-19), and then decomposing $|G(s)|^2$ into the product of G(s) and its complex conjugate.

In order to find a physically realizable filter that has the transfer function G(s), the poles p_1 and p_2 in (4-14) must both have real negative parts. As shown below this requirement places restrictions upon the constants b and c in (4-16). Suppose that $Q(s^2)$ in (4-19) is factorized to

$$Q(s^2) = (s^2 - r_1)(s^2 - r_2) \qquad (4\text{-}20)$$

and that each of the root factors in (4-20) is again factorized so that

$$Q(s^2) = R(s) = (s + \sqrt{r_1})(s - \sqrt{r_1})(s + \sqrt{r_2})(s - \sqrt{r_2}) \qquad (4\text{-}21)$$

The poles p_1 and p_2 in (4-14) must be chosen from among the four roots of R(s) as shown in (4-21). Thus at least two of the roots of R(s) in (4-21) must have negative real parts. If either r_1 or r_2 in (4-20) is non-positive real then two of the roots of R(s) are pure imaginary or zero, and only one of the remaining roots of R(s) can have a negative real part. If

both r_1 and r_2 are non-positive real, then there is no root of R(s) that has a real negative part. Therefore, physical realizability requires that r_1 and r_2 be both positive, or complex. This is done by proper choice of b and c. Since from (4-19)

$$Q(s^2) = 1 + \frac{|H(0)|^2}{N_0 \Delta} - bs^2 + cs^4$$

then by the quadratic formula

$$\left.\begin{matrix} f_1 \\ f_2 \end{matrix}\right\} = \frac{b}{2} \pm \sqrt{\left(\frac{b}{2}\right)^2 - \left(\frac{|H(0)|^2}{N_0 \Delta} + 1\right) c} \qquad (4\text{-}22)$$

we see that c must be positive for a physically realizable filter. If c is zero or negative then either r_1 or r_2 is zero or negative real, respectively. If, instead,

$$c \left(\frac{|H(0)|^2}{N_0 \Delta} + 1 \right) > \left(\frac{b}{2}\right)^2 \qquad (4\text{-}23)$$

then from (4-22), r_1 and r_2 are complex and therefore satisfactory. If (4-23) is not satisfied, but both b and c are positive, then from (4-22) r_1 and r_2 are both positive real and therefore satisfactory.

Positive real values of b and c have been found* which, when used in (4-16), yield an $|H_a(\omega)|^2$ which is a good approximation to $|H(\omega)|^2$. The zeroes z_1 and z_2 and the poles p_1 and p_2 are given in terms of the tape velocity V (in microinch/second) by

$$\begin{aligned} z_1 &= V e_1 \\ z_2 &= V e_2 \\ p_1 &= V f_1 \\ p_2 &= V f_2 \end{aligned} \qquad (4\text{-}24)$$

*See Appendices A and B.

The resulting values of e_1, e_2, f_1 and f_2, appropriate to the recording condition described in Table I below, are shown in Table II for different tape recorder signal-to-noise ratios. For each signal-to-noise ratio there is a different N_o. From (4-14), (4-19) and (4-24) we see that f_1 and f_2 vary with N_o and signal-to-noise ratio but that e_1 and e_2 do not, as indicated in the table.

Table I

Recording Conditions Assumed for Filter Computation

head-to-tape spacing	20 μin.
coating thickness	400 μin.
record gap length	150 μin.
reproduce gap length	25 μin.
deep gap field	1100 oe (¼ x sat. level)
tape switching fields	100/500 oe
tape permeabilities	5/2
multibit density	7500 bip (frequency doubling)

Table II

Transfer Function Poles and Zeroes

$e_1 = -0.002428 + j0$

$e_2 = -0.024203 + j0$

S/N	f_1	f_2
10 db	-0.01175 + j0	-0.02130 + j0
20 db	-0.02310 - j0.01542	-0.02310 + j0.01542
30 db	-0.03694 - j0.03270	-0.03694 + j0.03270
40 db	-0.06321 - j0.06082	-0.06321 + j0.06082

The relationship of these signal-to-noise ratios to the computer output has been explained previously (see p. 66, Final Development Report, 29 December 1967). For example, a signal-to-noise ratio of 40 db is

equivalent to a spectral noise "power" density (N_o) of 10^{-9} (units)^2/cycle at a tape speed of 10 ips. Since in the present computer program time and tape velocity are suppressed, the computation being made on the basis of tape distance in microinches, the 40 db signal-to-noise ratio noise density becomes 10^{-2}(units)^2 microinch. The 10 db figure is proportionately 10 (units)^2 microinch. At a bit density of 7500 the bit interval (Δ) is 133 microinch, and, therefore, the factors $N_o \Delta$ required in the filter design are respectively 1.33 and 1330 (units)^2 (microinch)^2.

4.3 7500 BPI Filtered Waveforms

For each signal-to-noise ratio there exist four distinct realizable circuits each having the required amplitude response, but differing phase responses. The phase response is governed by the selection of S-plane zeroes. The following scheme has been adopted:

Filter No.	Zeroes e_1	Zeroes e_2
1	-0.024203	-0.002428
2	-0.024203	+0.002428
3	-0.002428	+0.024203
4	+0.002428	+0.024203

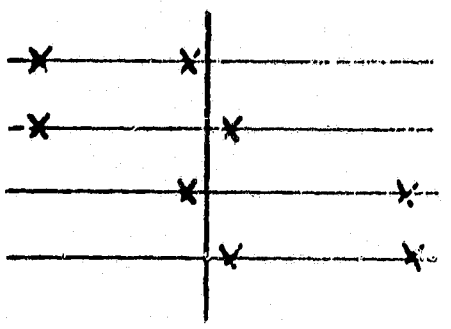

The sequence of figures is outlined below:

Fig. 13 Unfiltered single pulse and multibit waveform.

Fig. 14 S/N = 10 db
Fig. 15 S/N = 20 db
Fig. 16 S/N = 30 db
Fig. 17 S/N = 40 db

} Single and multibit for Filter 1

Figs. 18 - 21 same for Filter 2

Figs. 22 - 25 same for Filter 3

Figs. 26 - 29 same for Filter 4

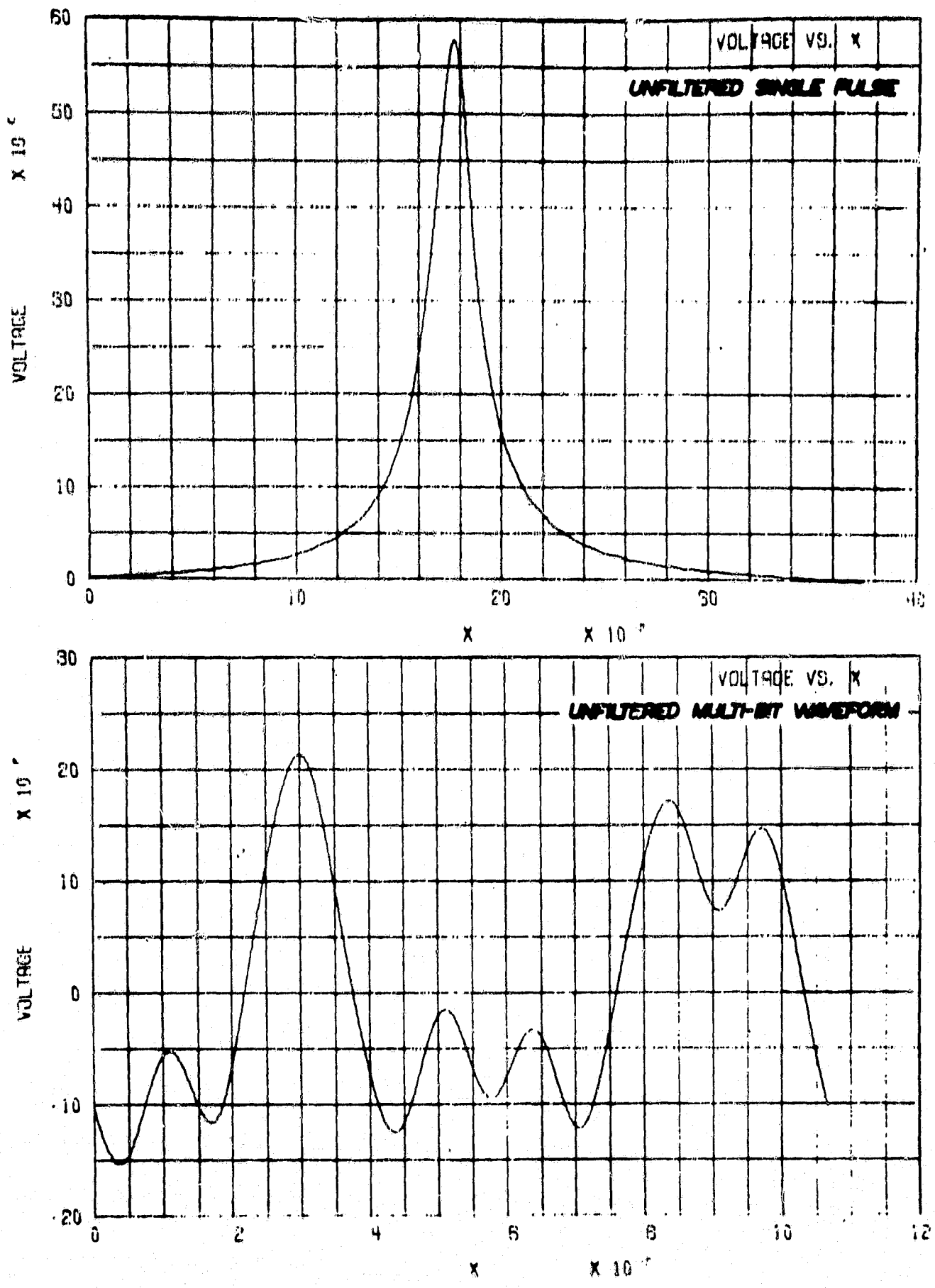

Fig. 13 Single Pulse and Multibit Waveform - Unfiltered

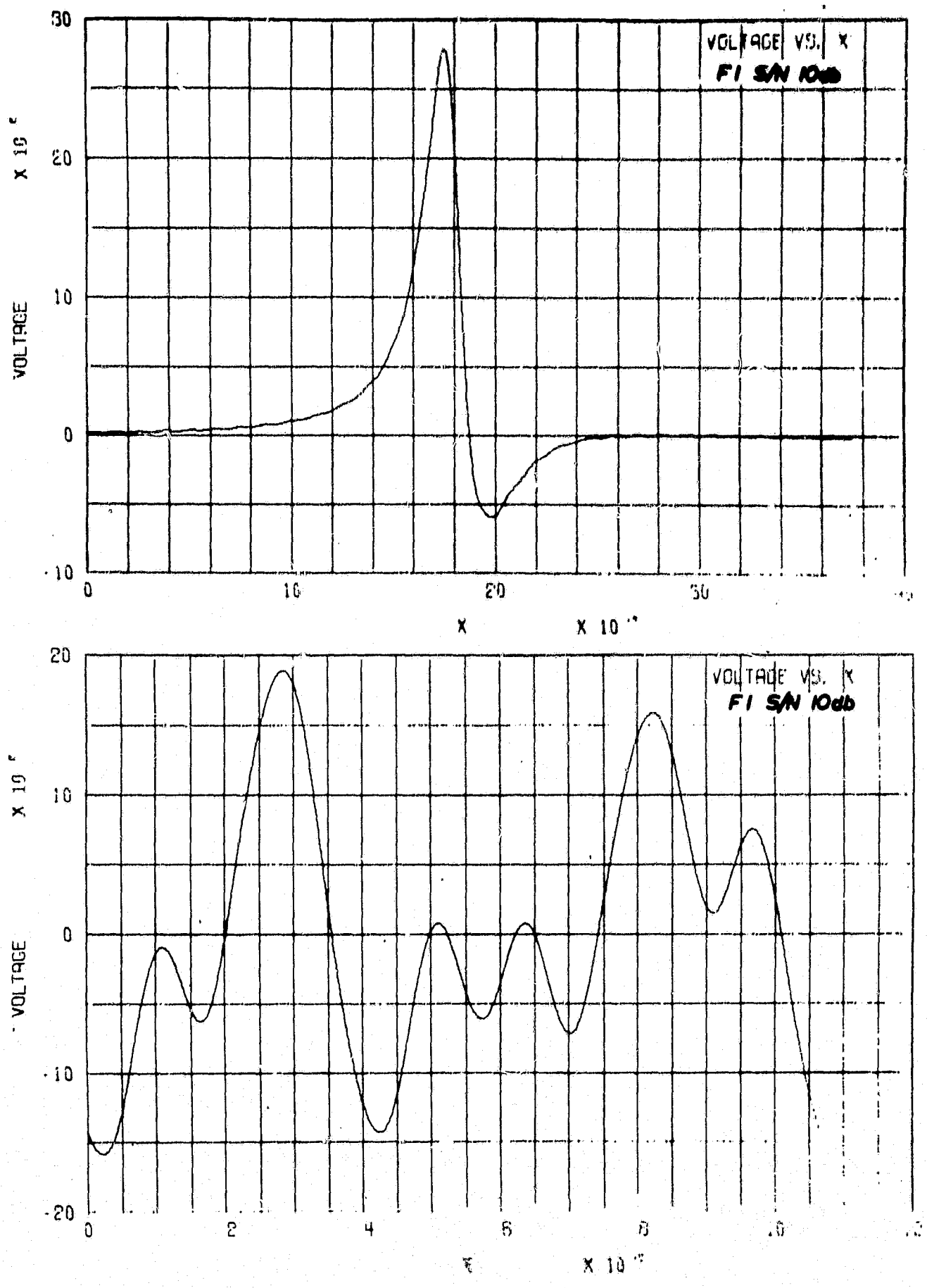

Fig. 14 Single Pulse and Multiple Waveform - Filter #1, S/N = 10 db

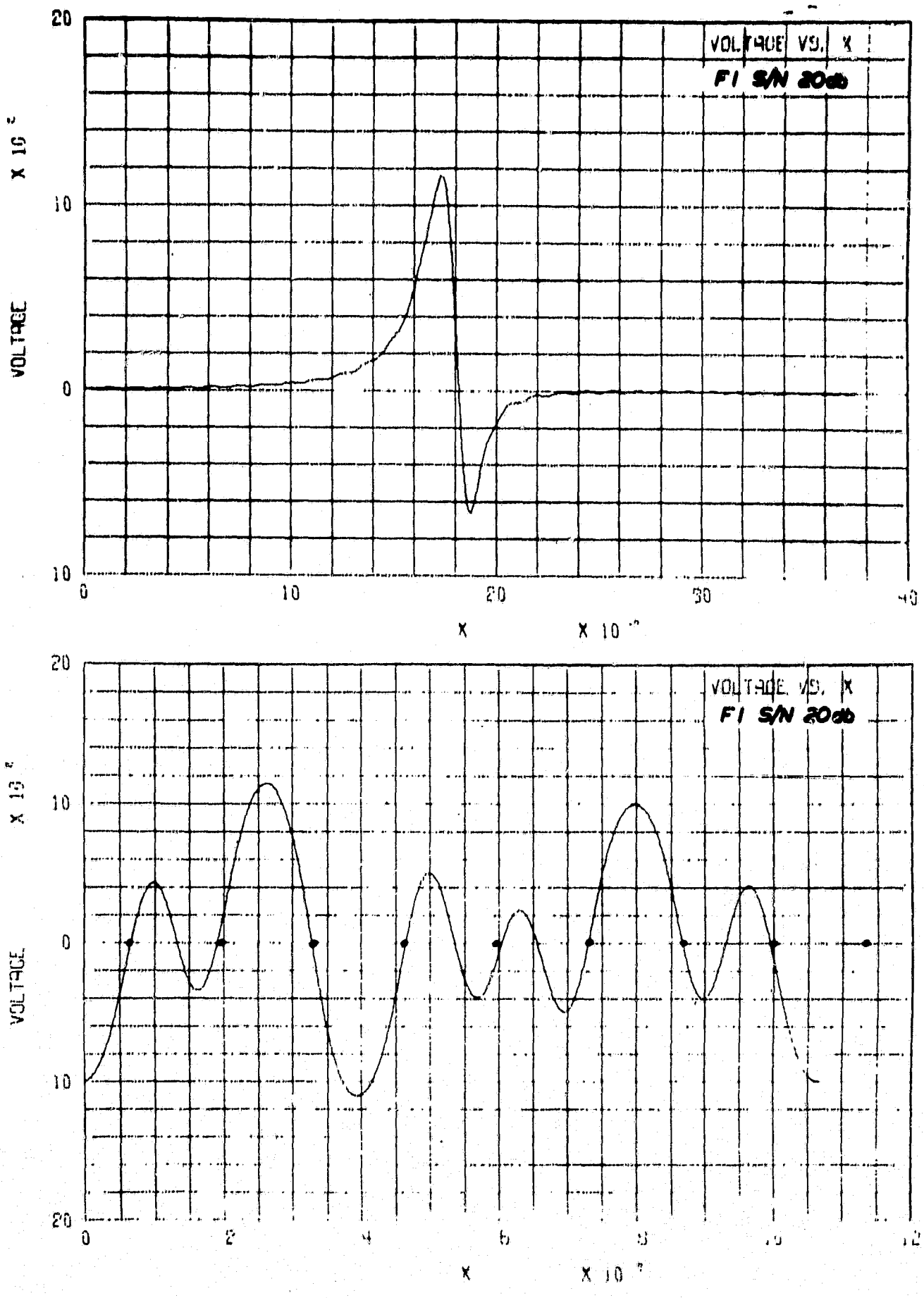

Fig. 15 Single Pulse and Multibit Waveform - Filter #1, S/N = 20 db

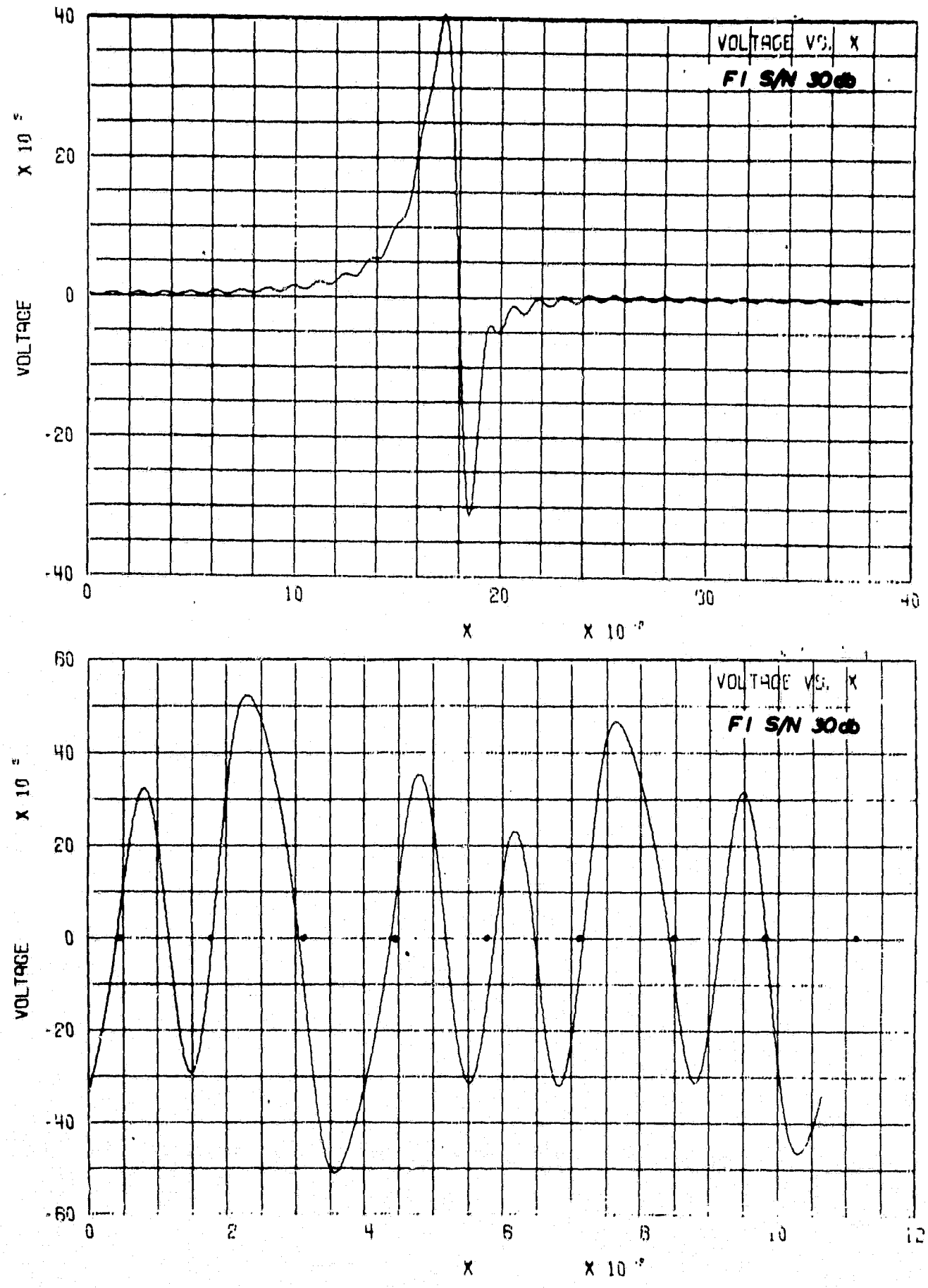

Fig. 16 Single Pulse and Multibit Waveform - Filter #1, S/N = 30 db

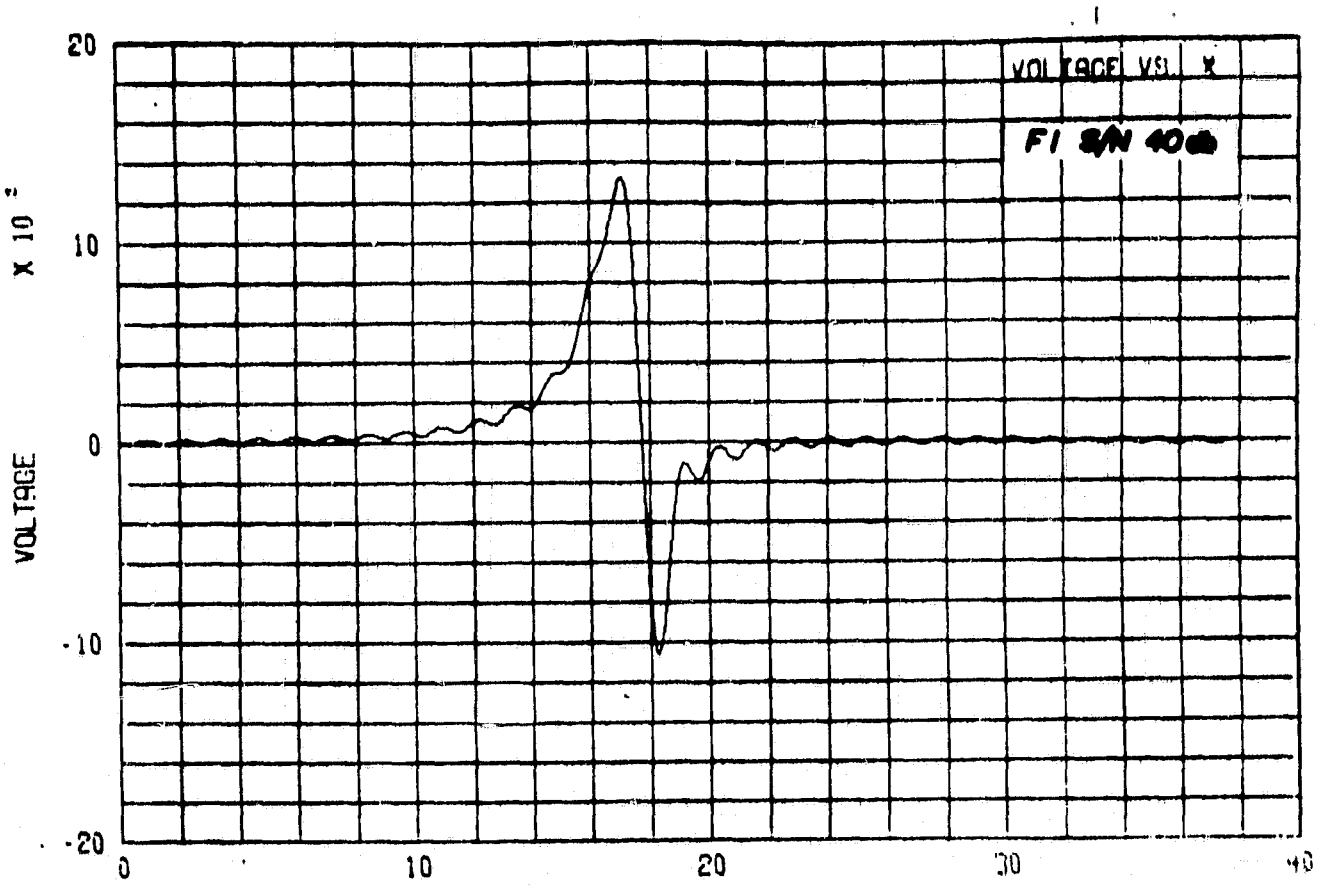

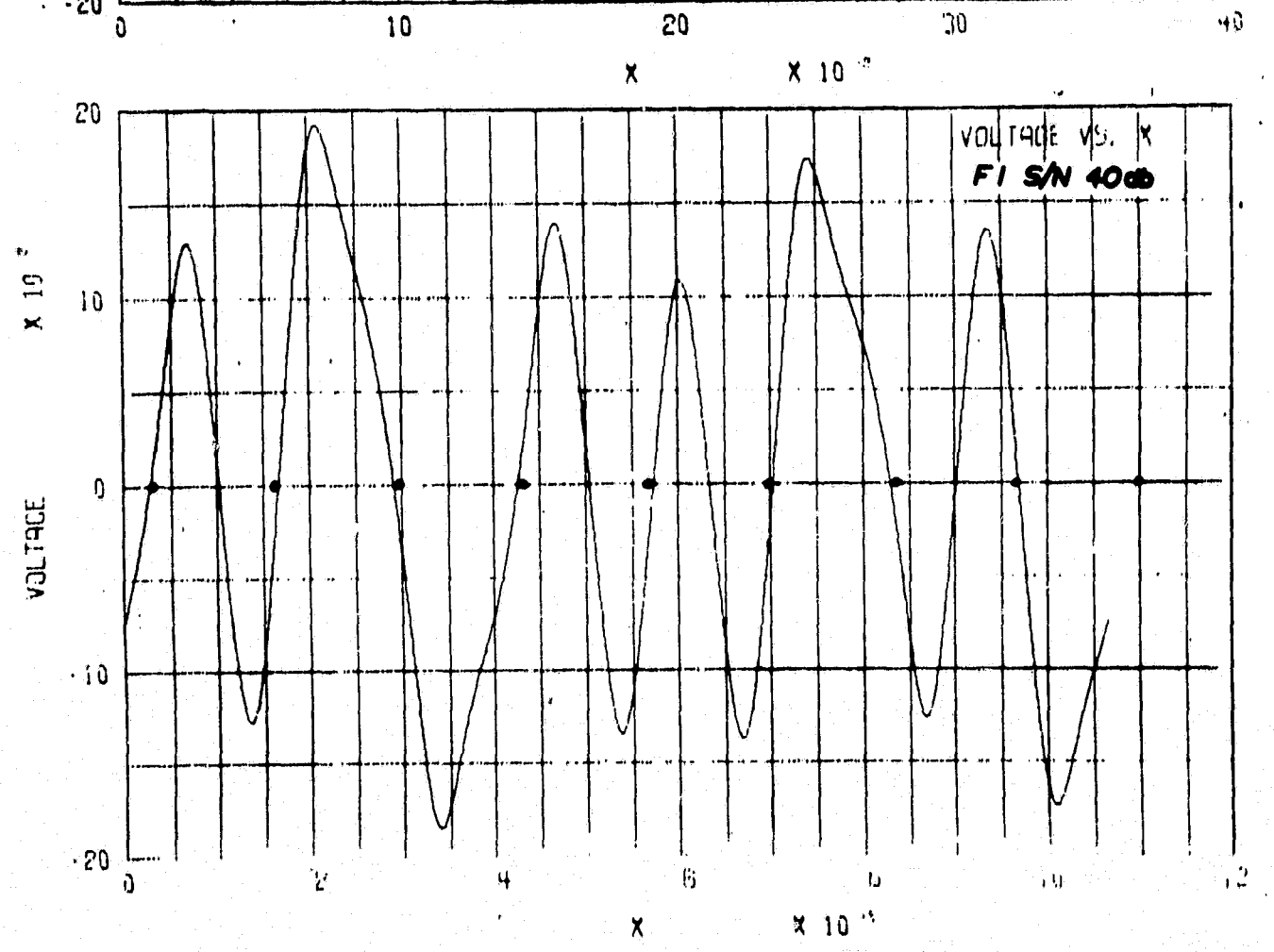

Fig. 17 Single Pulse and Multibit Waveform - Filter #1, S/N = 40 db

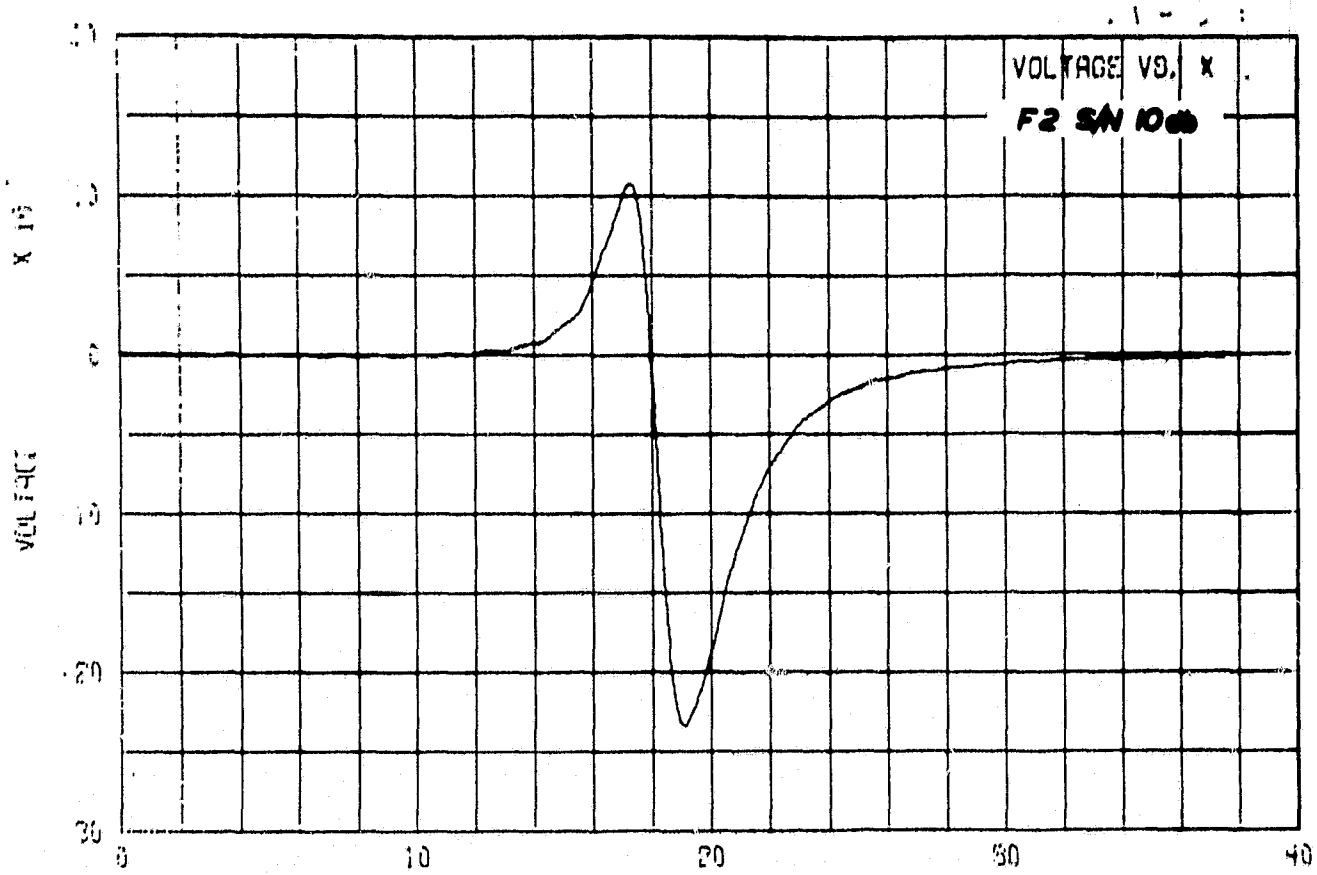

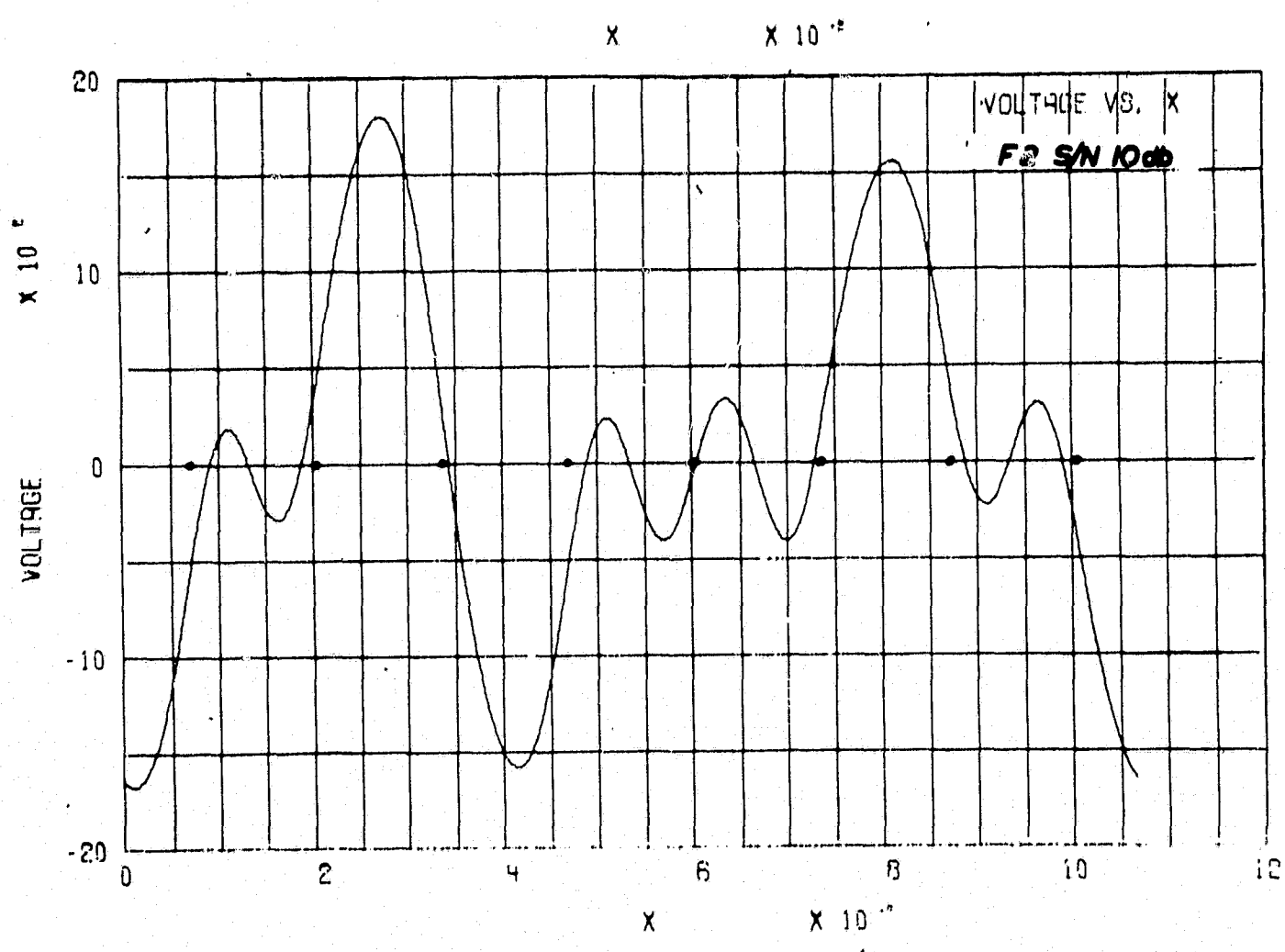

Fig. 18 Single Pulse and Multibit Waveform - Filter #2, S/N = 10 db

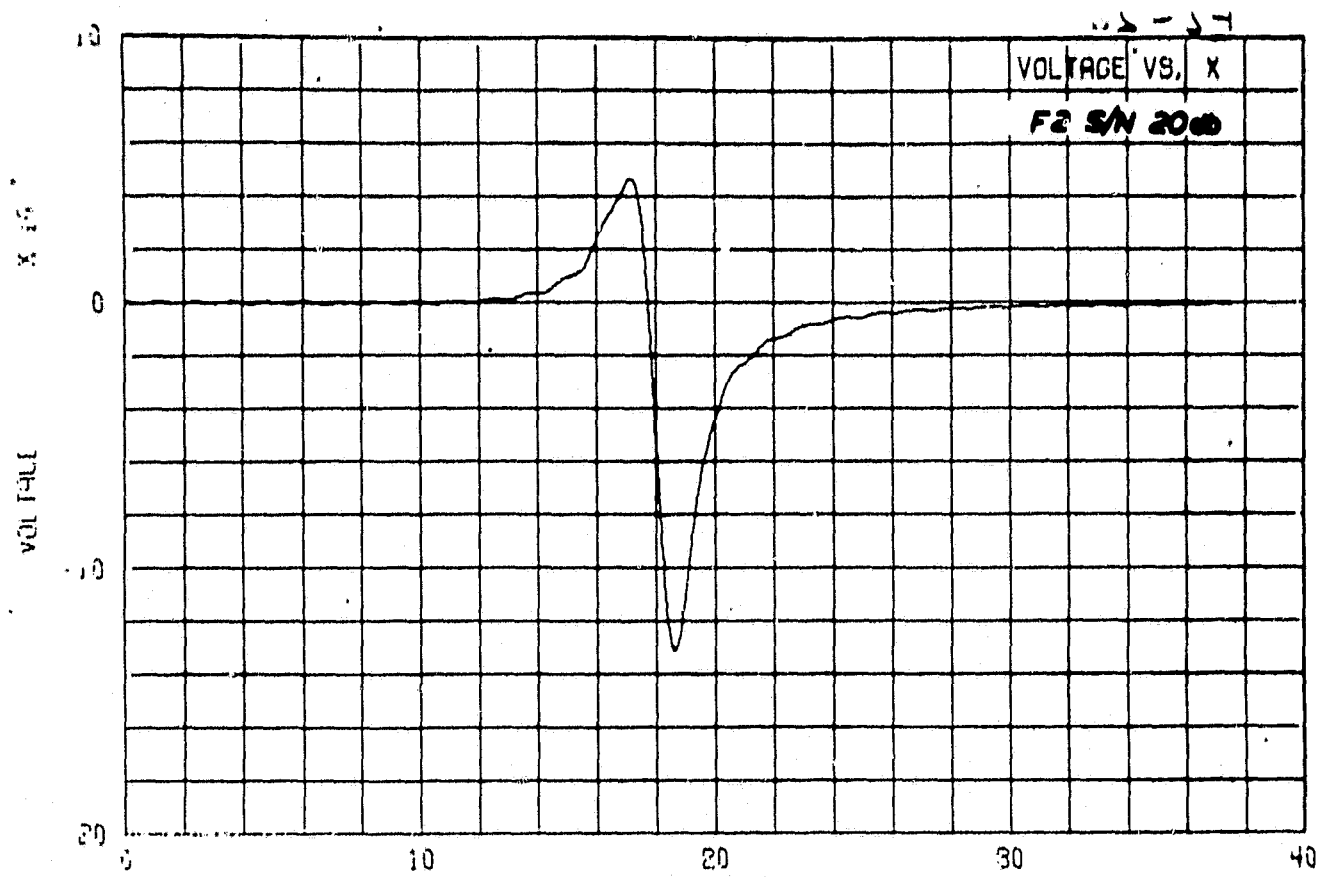

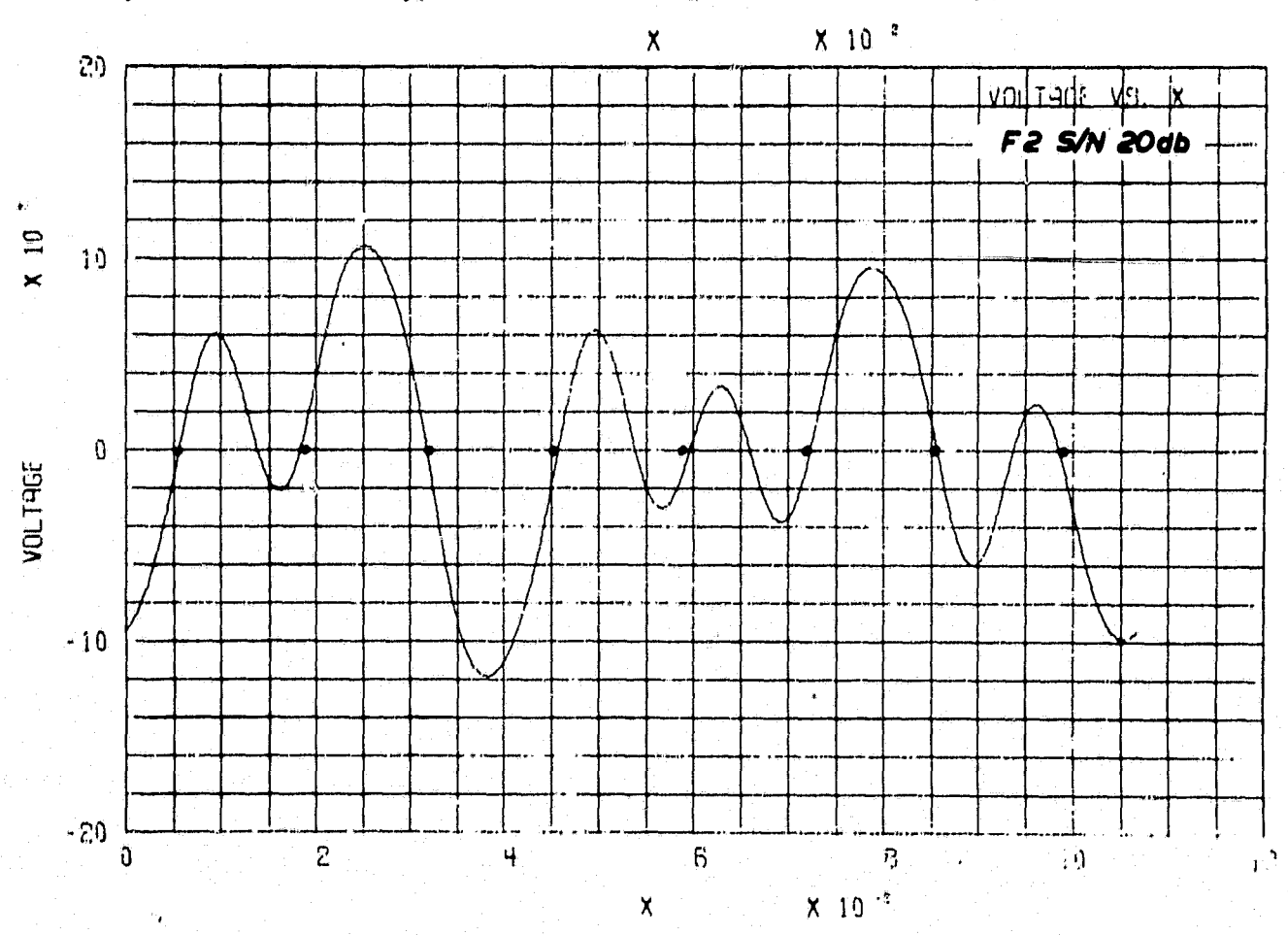

Fig. 19 Single Pulse and Multibit Waveform - Filter #2, S/N = 20 db

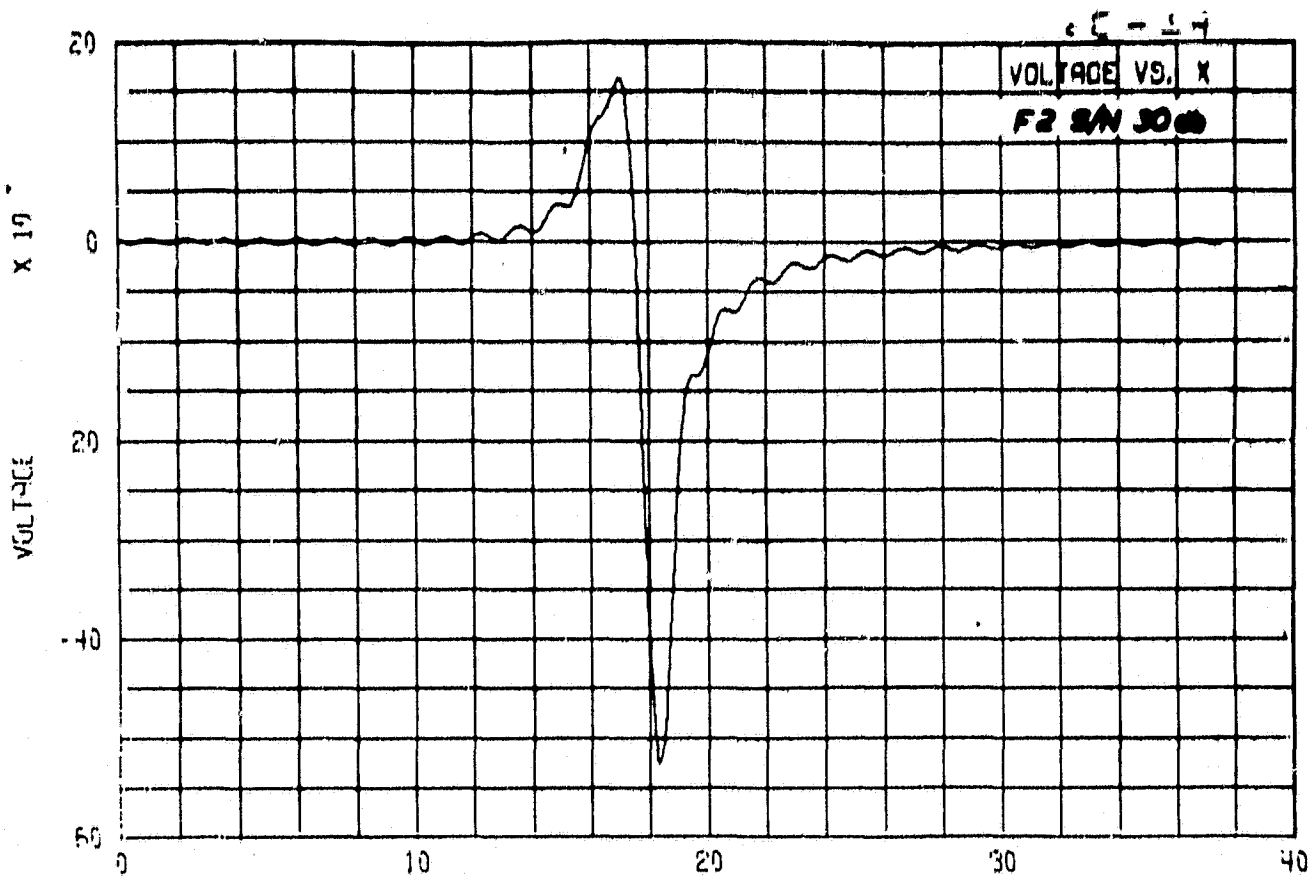

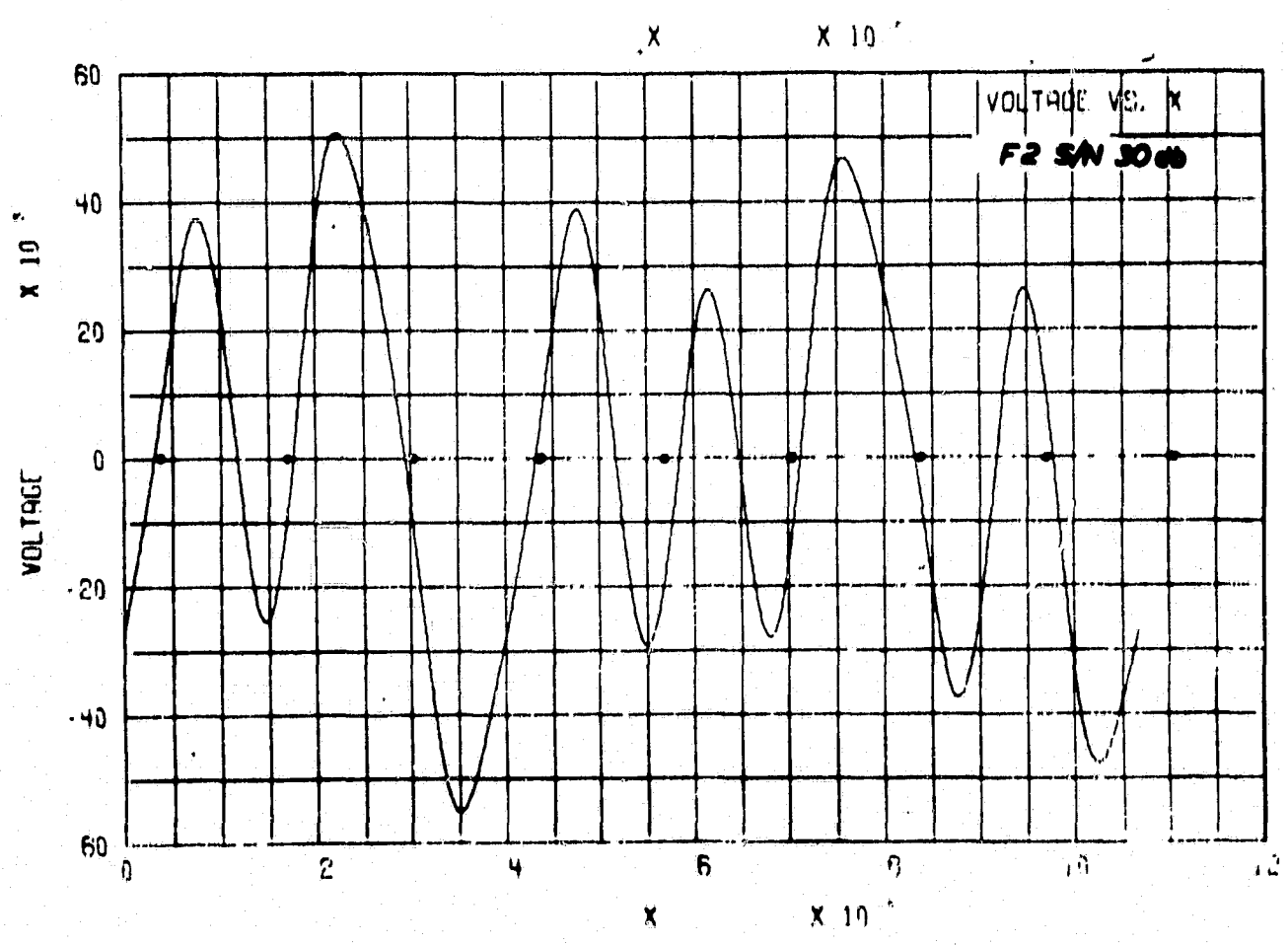

Fig. 20 Single Pulse and Multibit Waveform - Filter #2, S/N = 30 db

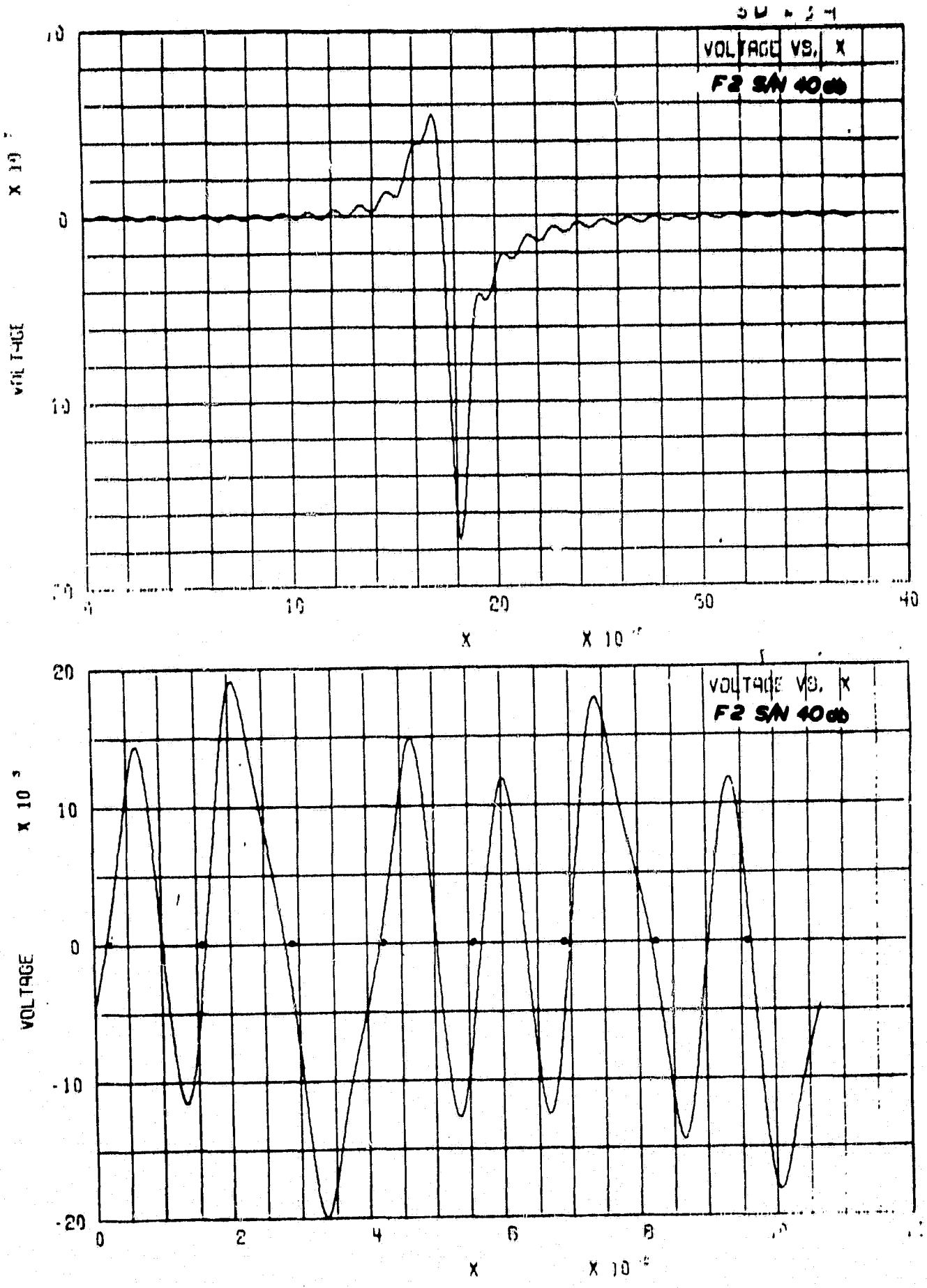

Fig. 21 Single Pulse and Multibit Waveform - Filter #2, S/N = 40 db

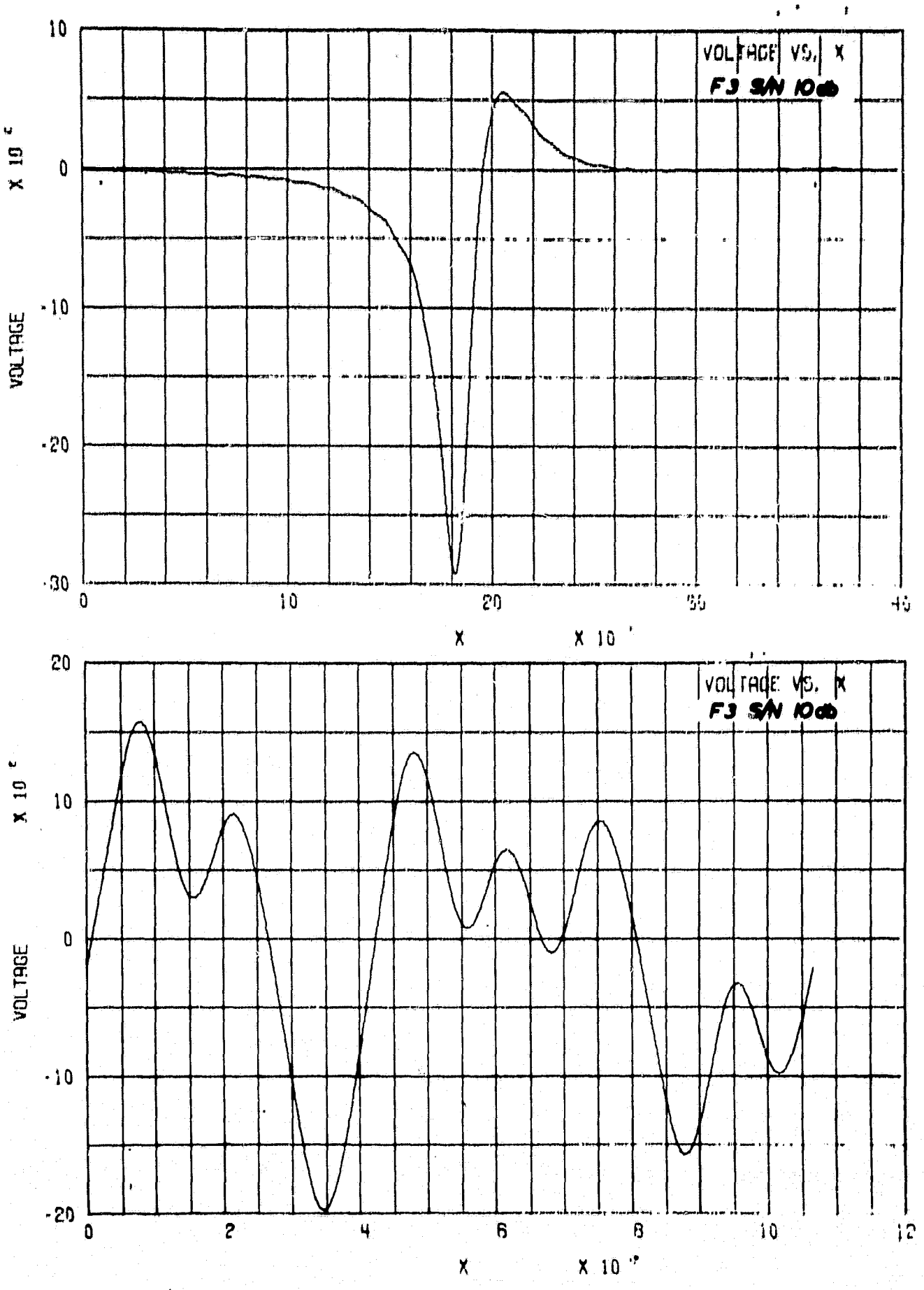

Fig. 22 Single Pulse and Multibit Waveform - Filter #3, S/N = 10 db

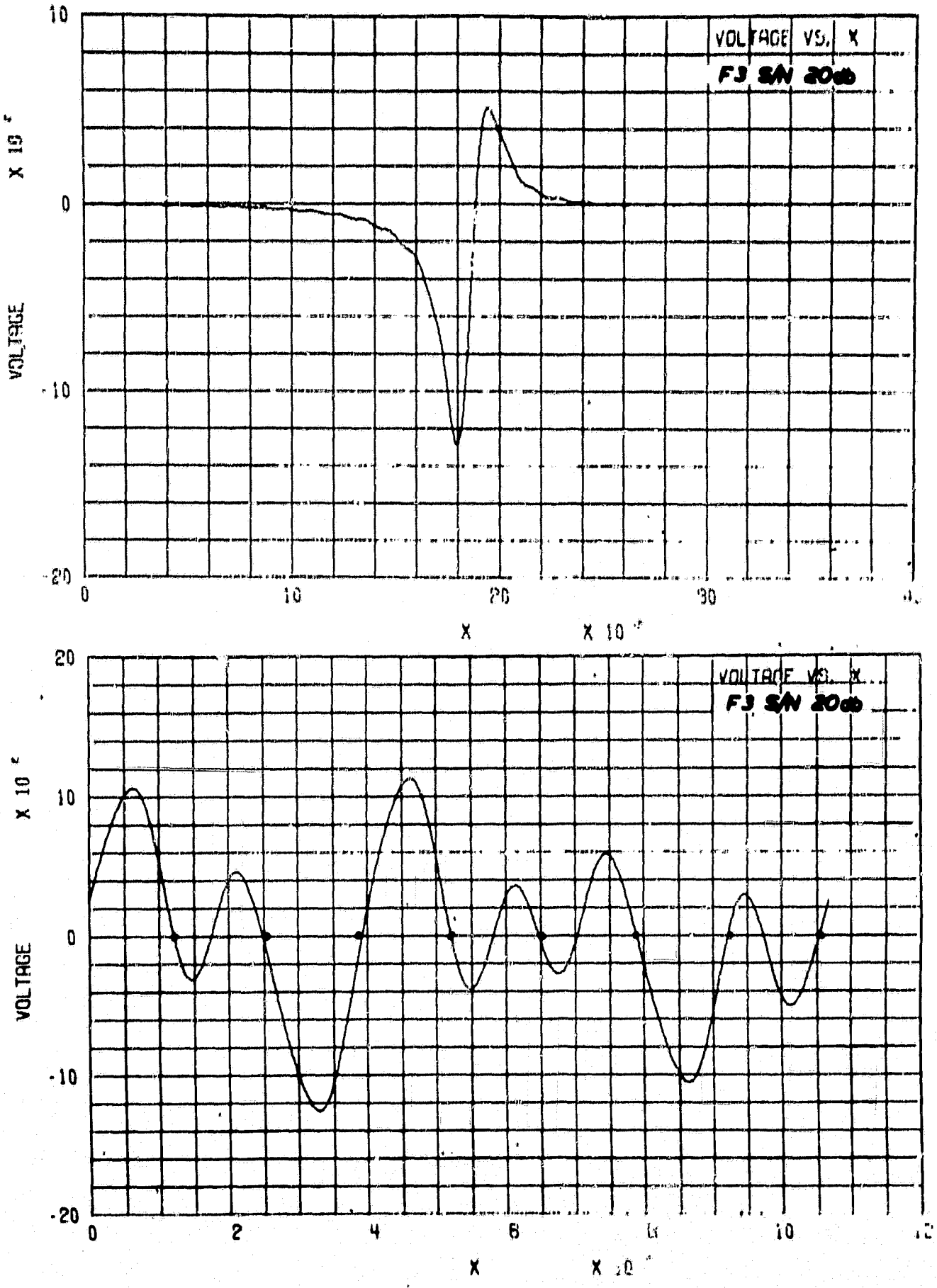

Fig. 23 Single Pulse and Multibit Waveform - Filter #3, S/N = 20 db

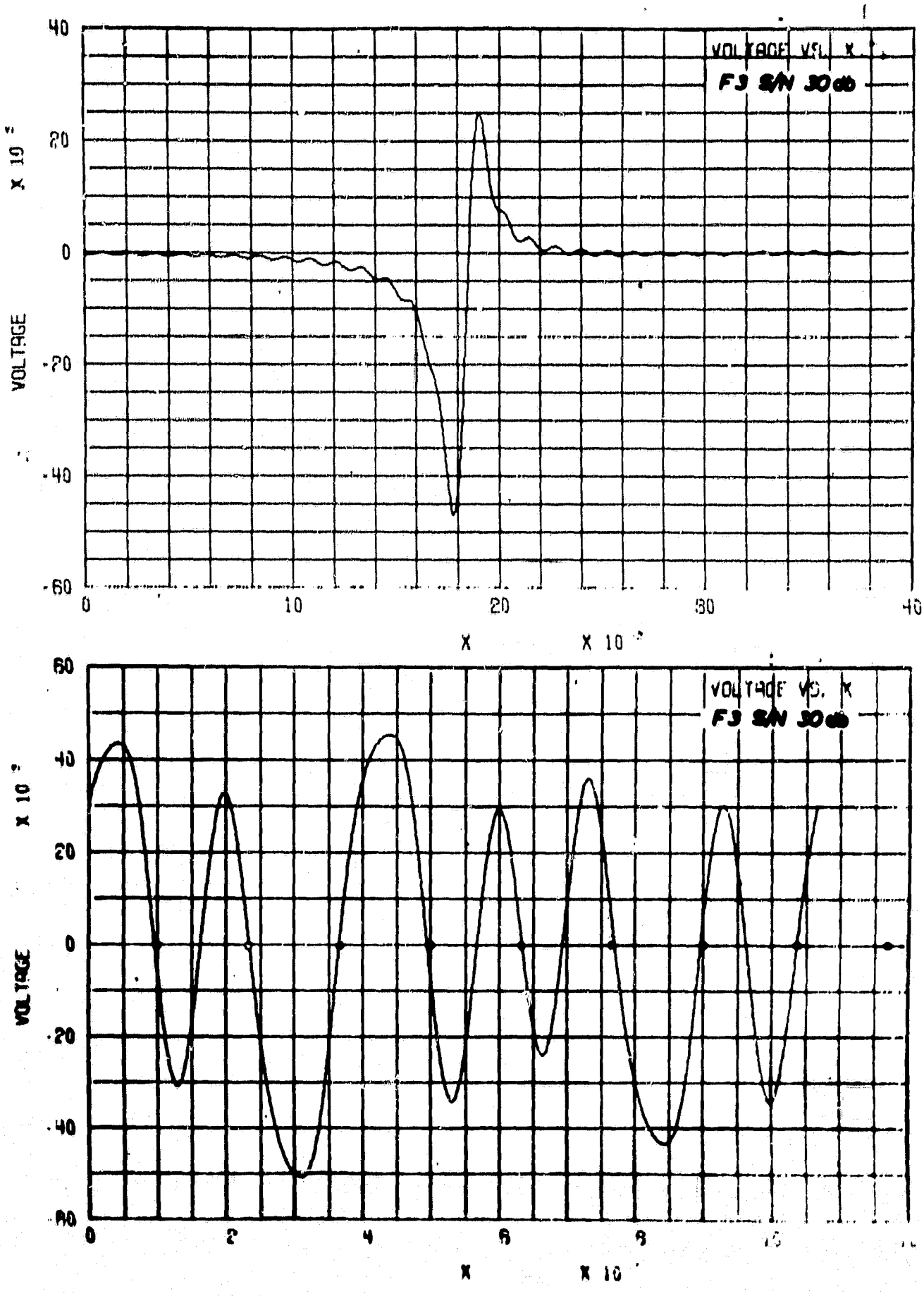

Fig. 24 Single Pulse and Multibit Waveform - Filter #3, S/N = 30 db

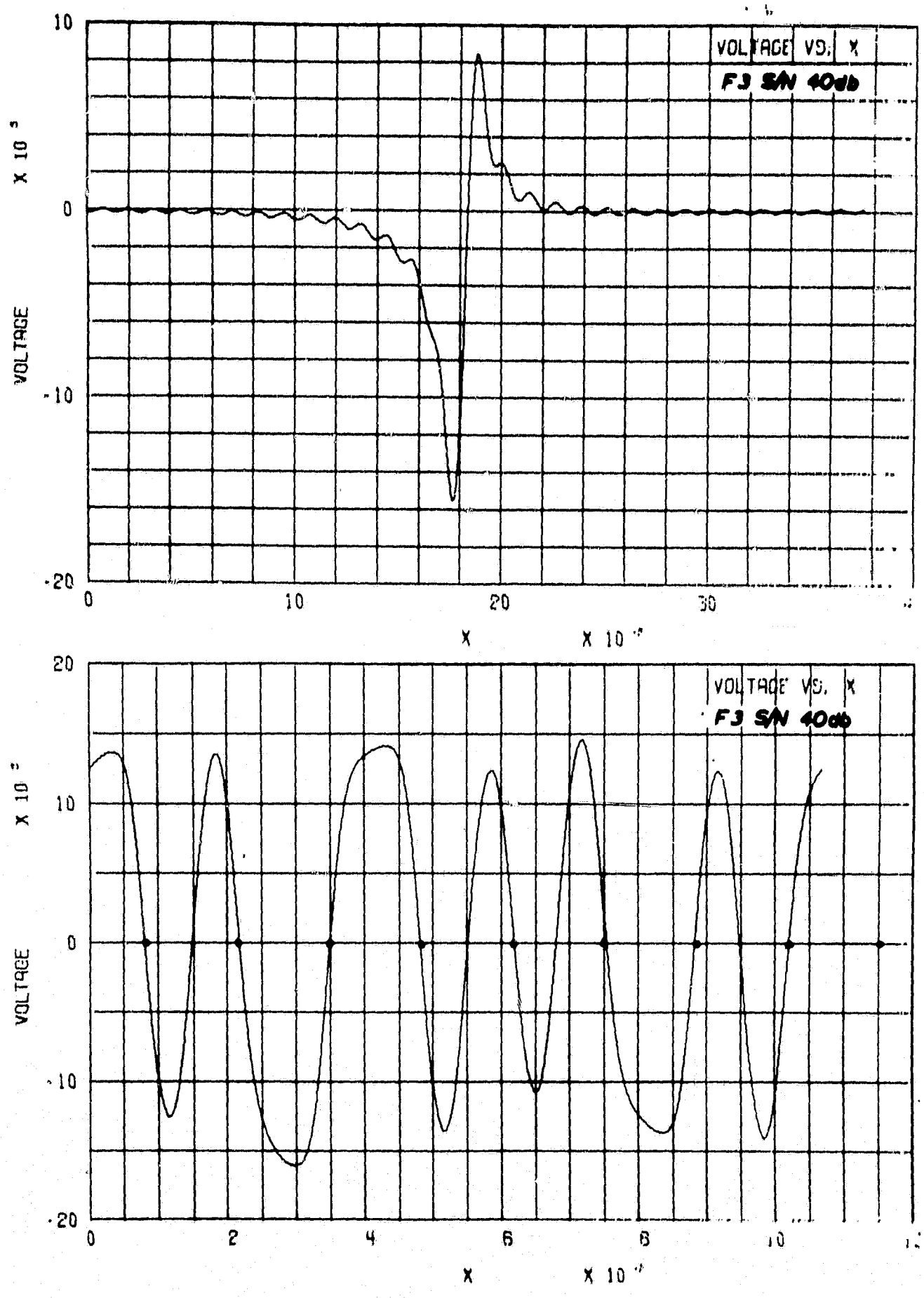

Fig. 25 Single Pulse and Multibit Waveform - Filter #3, S/N = 40 db

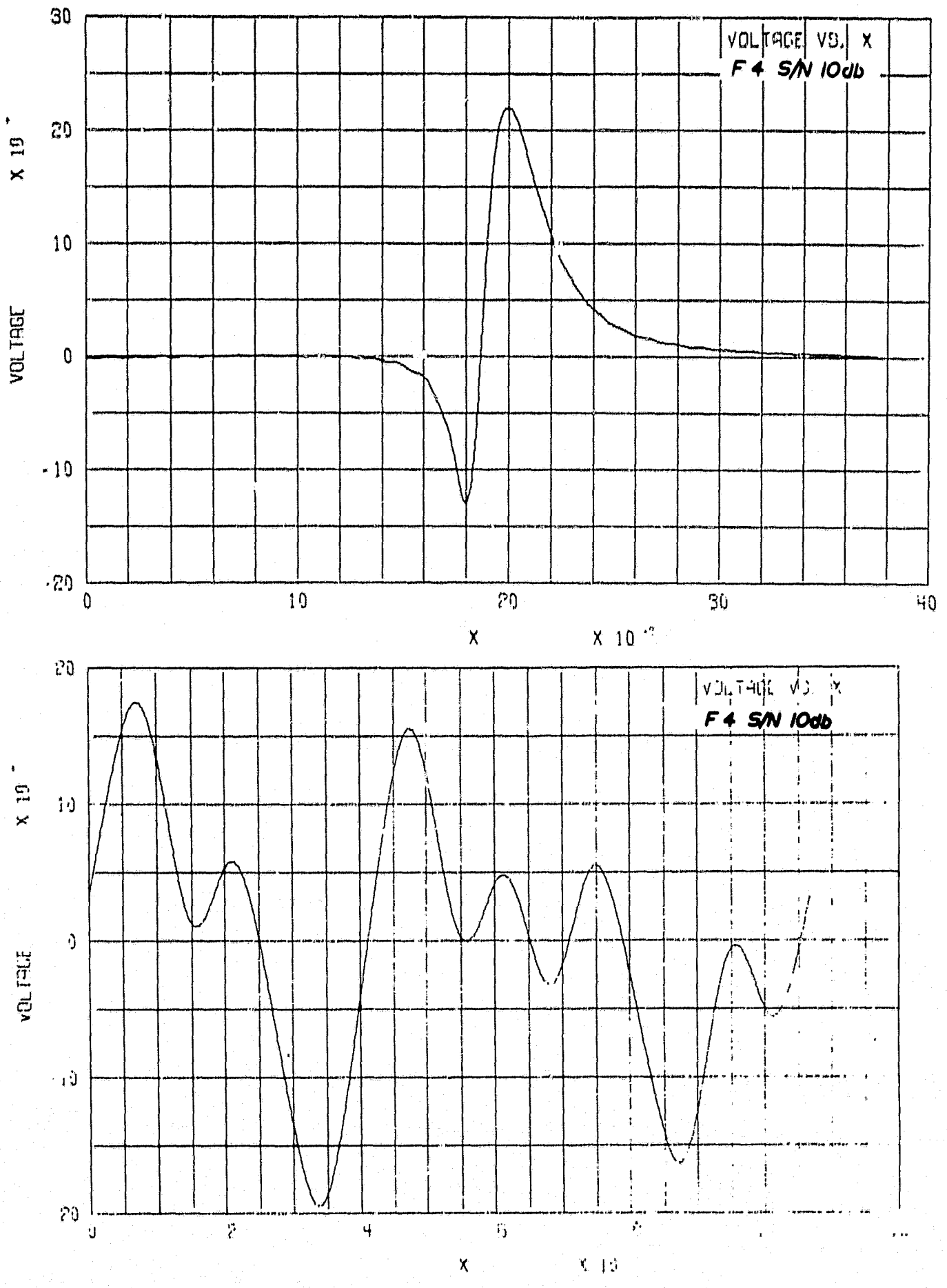

Fig. 26 Single Pulse and Multibit Waveform - Filter #4, S/N = 10 db

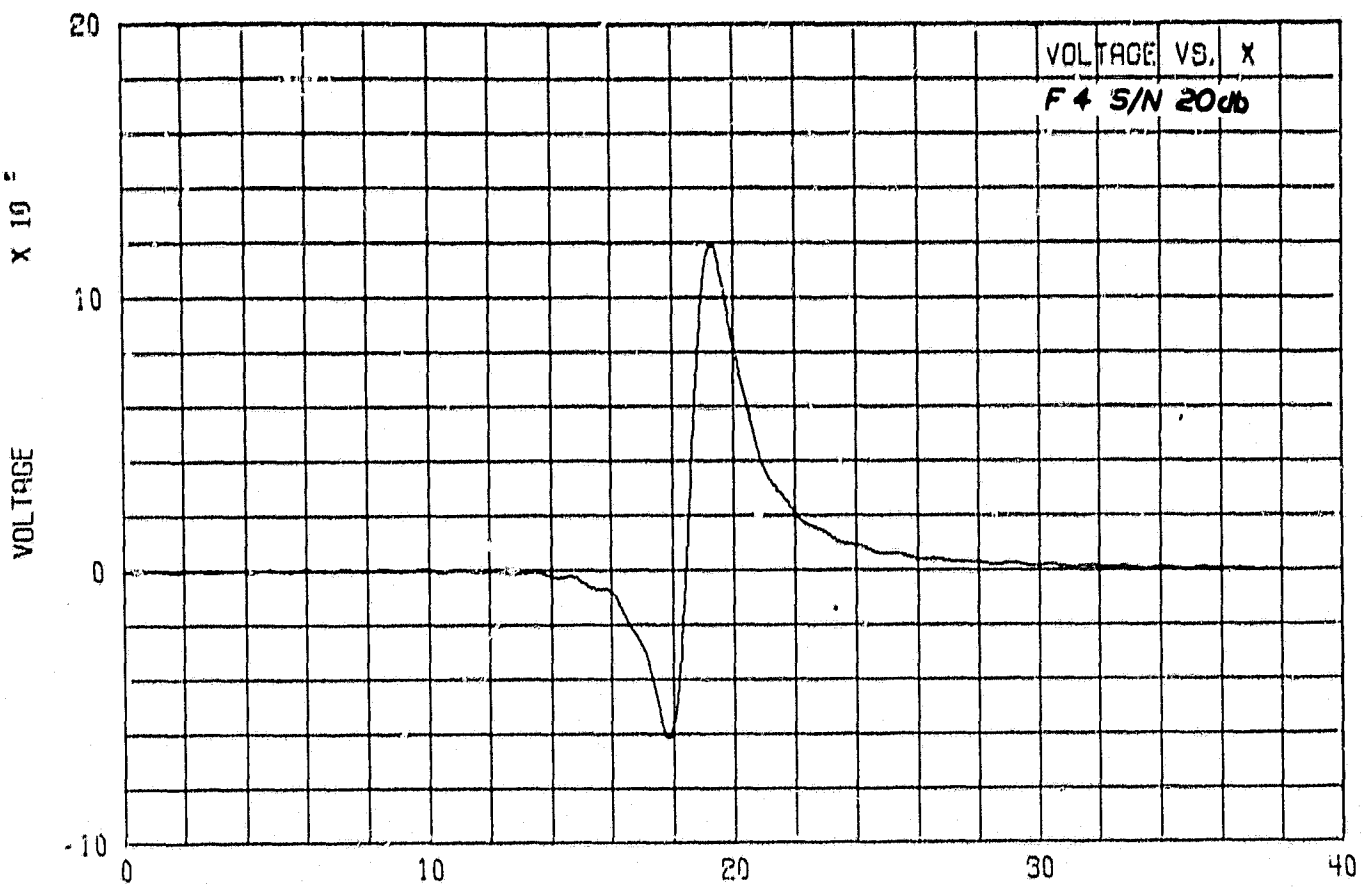

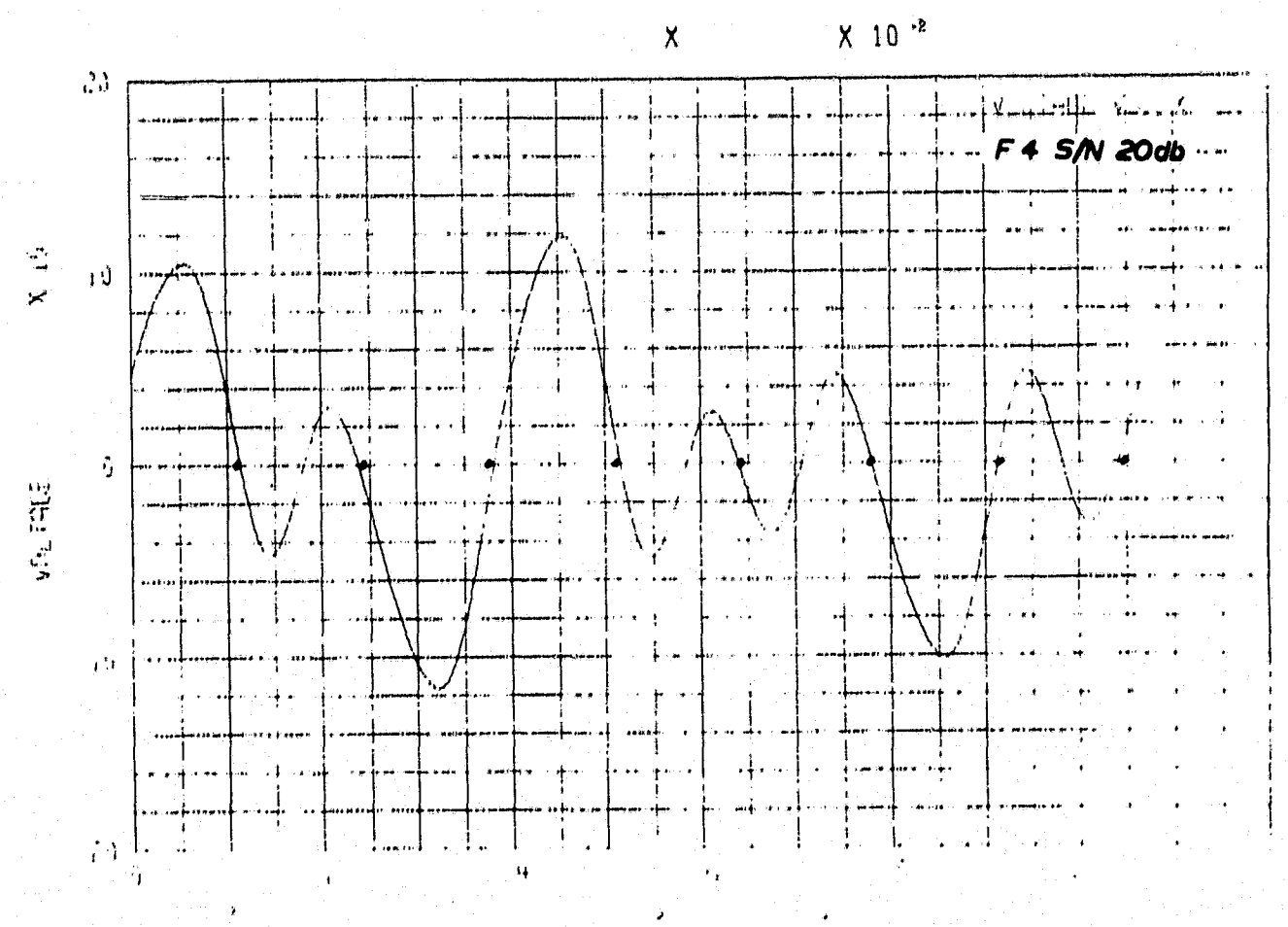

Fig. 27 Single Pulse and Multibit Waveform - Filter #4, S/N = 20 db

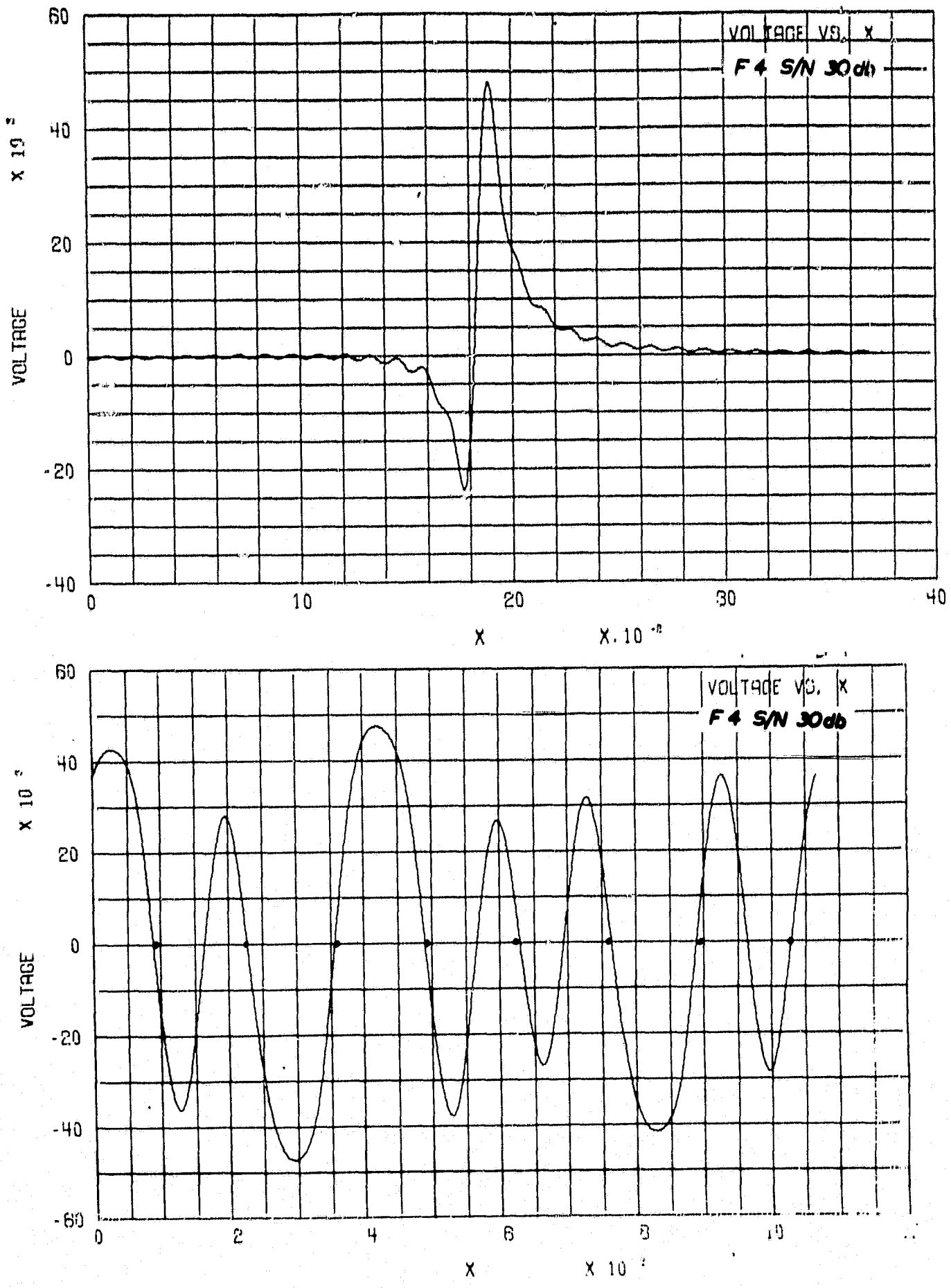

Fig. 28 Single Pulse and Multibit Waveform - Filter #4, S/N = 30 db

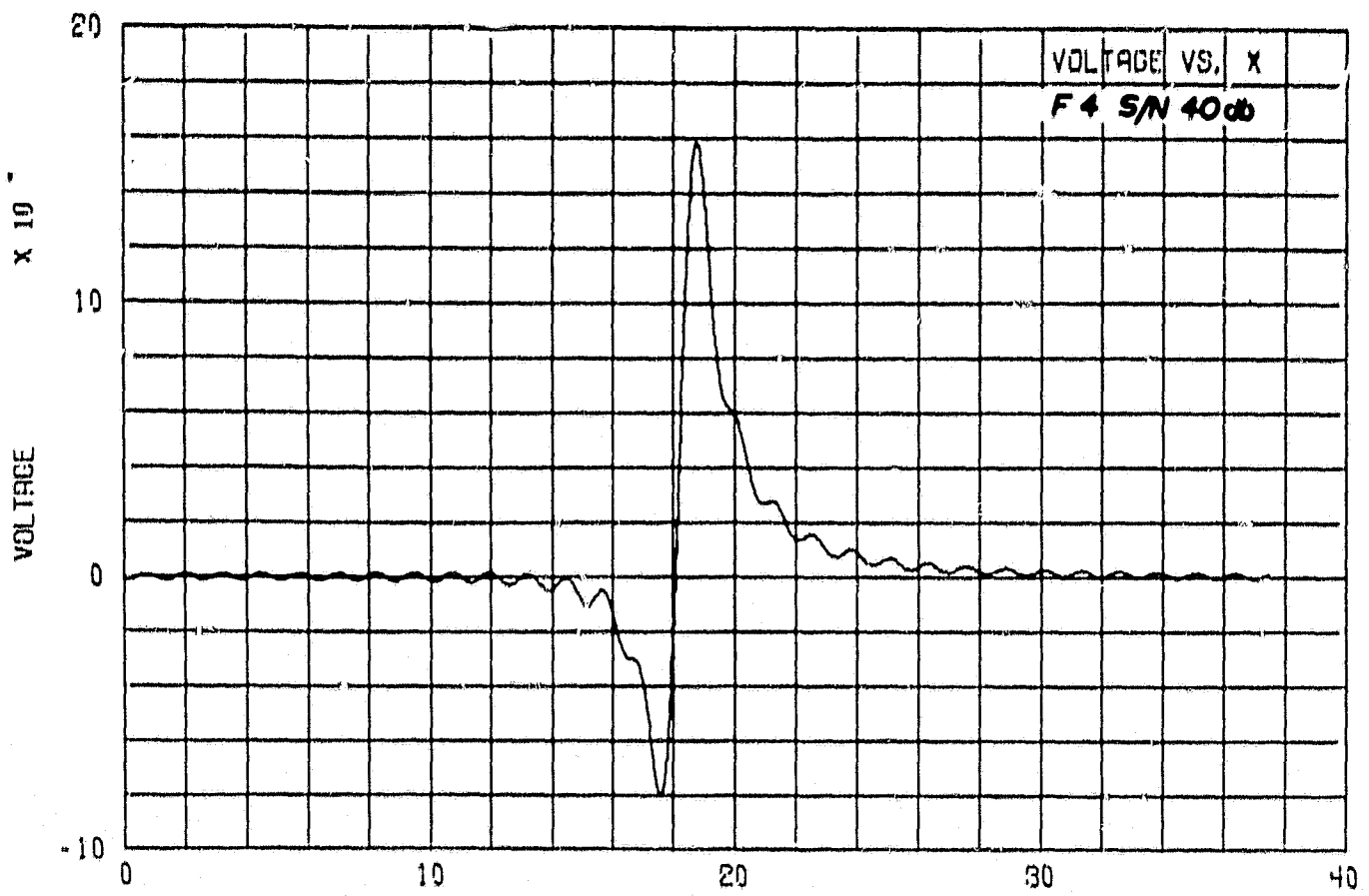

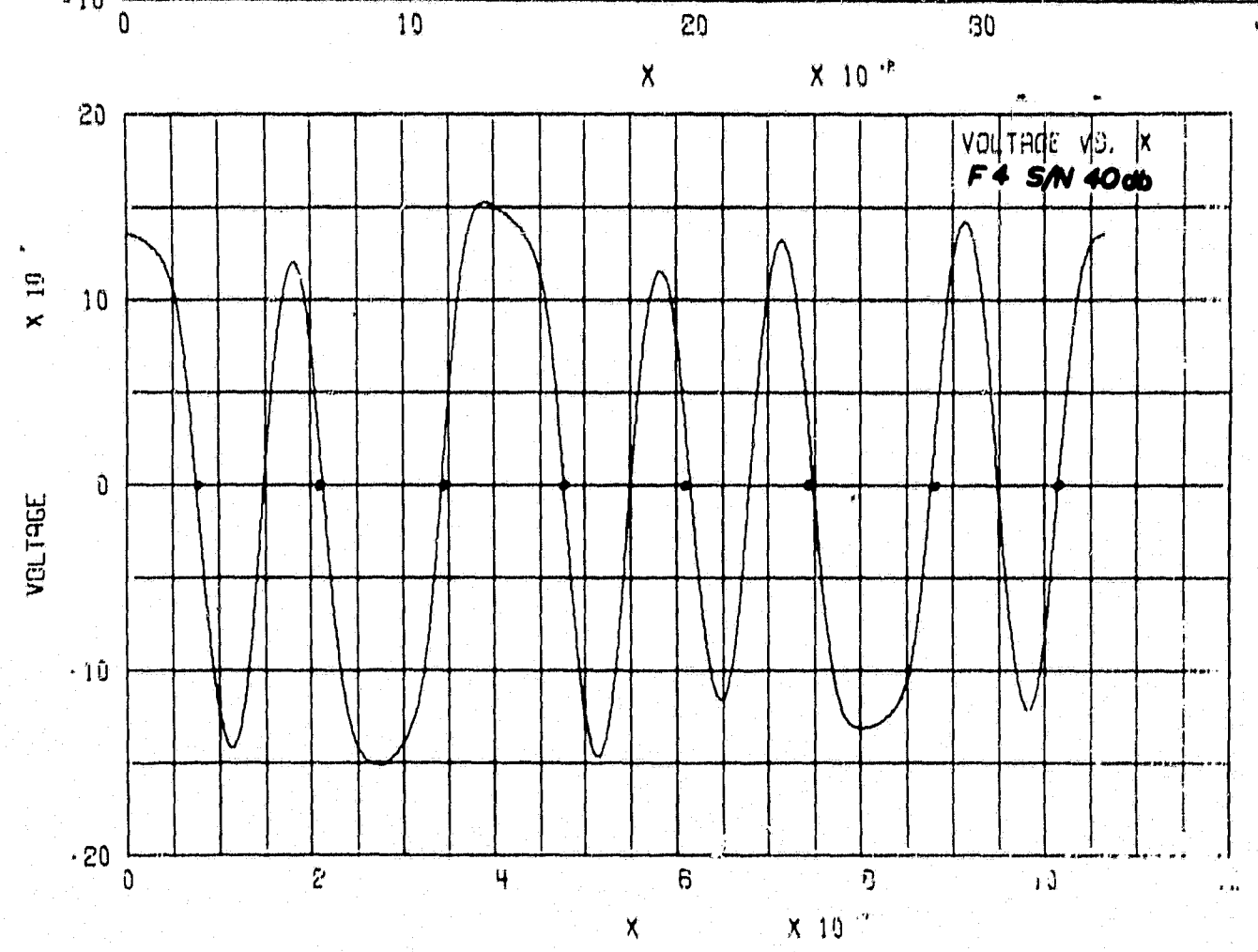

Fig. 29 Single Pulse and Multibit Waveform - Filter #4, S/N = 40 db

4.4 Constant Resistance Lattice Network Realizations

A constant resistance lattice network was chosen because it permits the realization of all four zero configurations in one simple network*.

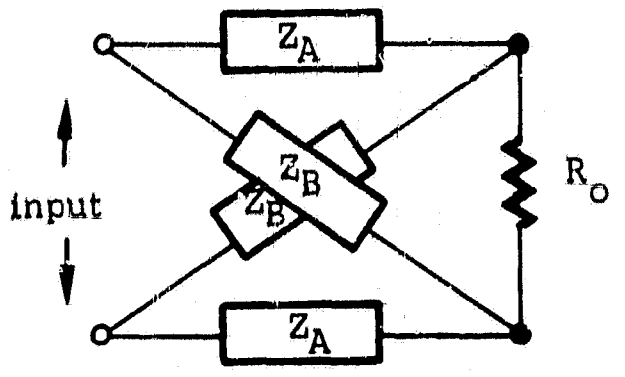

A terminating resistance of 50 ohms is assumed throughout the calculations.

The sections Z_A have the form:

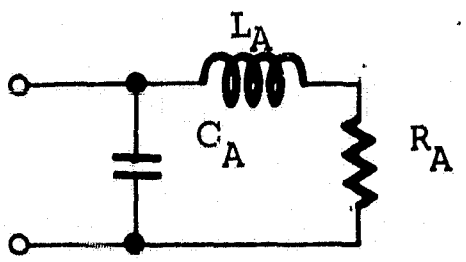

The sections Z_B have the form:

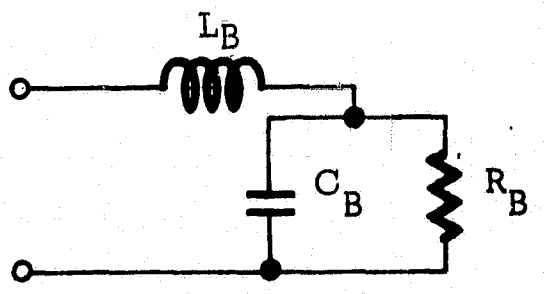

*The procedures adopted are explained in Appendix C.

A tape speed of 10 ips was adopted throughout this calculation and is valid in the component value table below. This tape speed is convenient because it matches that used in the signal-to-noise ratio determinations. Thus, 40 db corresponds to 100 x tape limited noise power, 20 db to 10,000 x tape limited noise power and etc.

At other tape speeds the component values may, of course, be scaled directly according to:

Inductance at V ips = Table value x 0.1 V

Resistance at V ips = Table value (no change)

Capacitance at V ips = Table value x 0.1 V

Throughout the table

L is in milli-henries (10^{-3} H)

R is in ohms (Ω)

C is in nano-farads (10^{-9} F)

Table III

(R_o = 50 ohms) (V = 10 IPS)

	S/N	L_A	R_A	C_A	L_B	R_B	C_B
Filter #1	10	100	31	620	1600	81	42
	20	120	43	200	510	58	47
	30	95	48	85	210	52	38
	40	64	49	40	100	51	26
Filter #2	10	290	81	350	890	31	120
	20	170	58	160	410	43	69
	30	110	52	77	190	48	44
	40	69	51	38	96	49	27

Table III (cont'd)

	S/N	L_A	R_A	C_A	L_B	R_B	C_B
Filter #3	10	1400	81	73	180	31	570
	20	480	58	59	150	43	190
	30	200	52	42	100	48	81
	40	97	51	27	67	49	39
Filter #4	10	970	31	67	170	81	390
	20	440	43	55	140	58	180
	30	200	48	40	99	52	81
	40	99	49	26	65	51	39

Eventually one of the zero combinations (i.e. filters) will be chosen as the most favorable one. Depending upon this selection it might be possible to find an even simpler network (e.g. ladder type). Every lattice network can be transformed into an unbalanced filter using a transformer, and sometimes reduction is possible without transformer coupling*. Given a specific zero combination, an active network approach could yield the least space consuming and simplest filter.

4.5 Some General Observations

There exists little difference between the performance of the four filters. Some slight trends only are evident; for example, only FILTER #2 was able to correct all the zero crossings at 10 db S/N, and FILTER #3 and FILTER #4 show nearly equal one and zero signal amplitudes at the high S/N whereas FILTERS #1 and #2 do not. However, it is presently felt that these slight differences are of no great importance.

*See for example, J. E. Storer, "Passive Network Synthesis", McGraw-Hill, 1957.

Similarly it would appear that no one filter is particularly preferable from the point of view of the network component values required. Thus it seems clear that the eventual choice cannot be determined by present considerations. The type of detector which is chosen to follow the "noise-whitening" filter may well influence the choice.

It may be observed, from the computer filtered waveforms, that the principal effect of high signal-to-noise ratio filters is to reduce the effects of pulse crowding. Specifically, there remains but little evidence of bit shift and all the zero crossings are present. Approximately, the effective bit density is reduced by a factor of at least four. Thus the filtered 7500 bpi waveform is similar to an unfiltered 2000 bpi waveform. The price paid is, of course, attenuation of the signal. In the 40 db S/N ratio cases, all four filters attenuated the multibit waveform by a factor of about 10 -- a 20 db signal loss. It is interesting to note that the attenuation in isolated pulse peak amplitude is greater than this. The frequency-doubling multibit waveform automatically excludes much of the low frequency (large wavenumber) information present in the isolated pulses.

Approximate "paper" calculations, assuming that the isolated pulse can be represented by a bi-exponential, lead to the conclusion that, at high signal-to-noise ratios, the effect of the noise-whitening filter is to reduce the signal amplitude to the square root of its unfiltered amplitude. Thus the signal-to-noise ratio figure in decibels will be halved. This reduction is very close to that seen in the computed waveforms.

5.0 CONCLUSIONS

1) The present computer program, which uses a non-interacting model for tape remanent magnetization is exactly equivalent to the "pseudo-linearity" add-up process provided only that the record head field shows step transitions (of negligible rise distance compared to the bit interval).

Further, since the existing program has been shown, by direct experimental validation, to be applicable from the lowest bit densities to at least 15,000 bpi when using γFe_2O_3 tape "in contact", it may be presumed that the linear addition of experimental pulses would also yield the correct multibit waveforms.

2) The principal factors governing the single transition output voltage waveform are understood. For high resolution systems (i.e. those with both small reproduce gap widths and head-to-tape spacing) the two most important factors are the coating thickness (d) (or depth of penetration) and the effects of demagnetization.

3) Given the validity of "pseudo-linearity", the problem of unscrambling the deleterious effect of pulse crowding and overlap becomes amendable to analysis by linear filter theory.

It has been demonstrated that the required linear filter is of the "noise-whitening" type as is used, typically, as a precursor to an optimum filter. Interestingly, this "noise-whitening" filter has many of the characteristics of a pulse "compressing" filter.

4) "Noise-whitening" filters having the correct amplitude transfer function have been designed which have different phase responses. The particular phase response does not appear to be critical since the computed filtered multibit waveforms show only slight differences. All filters can be realized with symmetrical 12 element passive lattice networks and simpler networks may be possible in special cases.

5) The effect of the filters is, as was expected, most pronounced at high signal-to-noise ratios, where the effective bit density is reduced by a factor of at least four. Nearly all bit shift disappears and all zero crossings are restored. The cost of these improvements is a halving of the decibel signal-to-noise ratio.

6) Very considerable progress has been made towards what promises to be the first rationally designed system of high density ($\approx$10 - 20,000 frpi) recording.

APPENDIX A

APPROXIMATION OF THE PULSE POWER SPECTRUM

In section 4.2, the development of the filter transfer of the output pulse shape h(t) was approximated by $|H_a(\omega)|^2$ given by

$$|H_a(\omega)|^2 = \frac{|H(0)|^2}{1 + b\omega^2 + c\omega^4} \tag{A-1}$$

by appropriate choice of the real constants b and c. Below we describe the procedure adapted for the choice of b and c.

Let

$$\delta = \left[|H(\omega)|^2 - |H_a(\omega)|^2\right]\left[1 + b\omega^2 + c\omega^4\right] \tag{A-2}$$

and combine this equation with (A-1) to give

$$\left[\omega^2 |H(\omega)|^2\right] b + \left[\omega^4 |H(\omega)|^2\right] c = |H(0)|^2 - |H(\omega)|^2 + \delta \tag{A-3}$$

We choose a total of n equally spaced frequencies ω_k, $1 \leq k \leq n$ with $n \geq 2$ and for each frequency, we use Eq. (A-3). Since these equations are linear in b and c we have a system of n linear equation that can be written in the matrix vector form

$$AX = d + \Delta \tag{A-4}$$

where A is a $n \times 2$ matrix with elements

$$a_{k1} = \omega_k^2 |H(\omega_k)|^2$$
$$a_{k2} = \omega_k^4 |H(\omega_k)|^2 \tag{A-5}$$

X is a two dimensional vector having elements b and c , d is an n element vector having elements

$$d_k = |H(0)|^2 - |H(\omega_k)|^2 \qquad \text{(A-6)}$$

and Δ is an n dimensional vector having elements δ_k . We find the vector X (or values b and c) that solves the second order linear system

$$A^T A X = A^T d \qquad \text{(A-7)}$$

It is shown in Appendix B that this solution minimizes the quantity

$$\sum_{k=1}^{n} \delta_k^2$$

As a matter of convenience, the power spectral density and the approximation to it were first computed as functions of $k = 2\pi/\lambda$ where λ is a wavelength on the tape, and later converted to functions of the frequency. This also facilitates adaptation to different tape speeds. Figures A-1 and A-2 show the power spectral density $|H(k)|^2$ and the approximation to it $|H_a(k)|^2$. To compute the value of b and c (see equation A-1), n was set equal to 3 . Matching was done at the three values of k shown in Figs. A-1 and A-2. In the computer program, the power spectral density curve of a single output pulse was approximated from the coefficients of a Fourier series that represents a periodic sequence of these pulses. The flat top on the curve of Fig. A-1 is a consequence of this approximation.

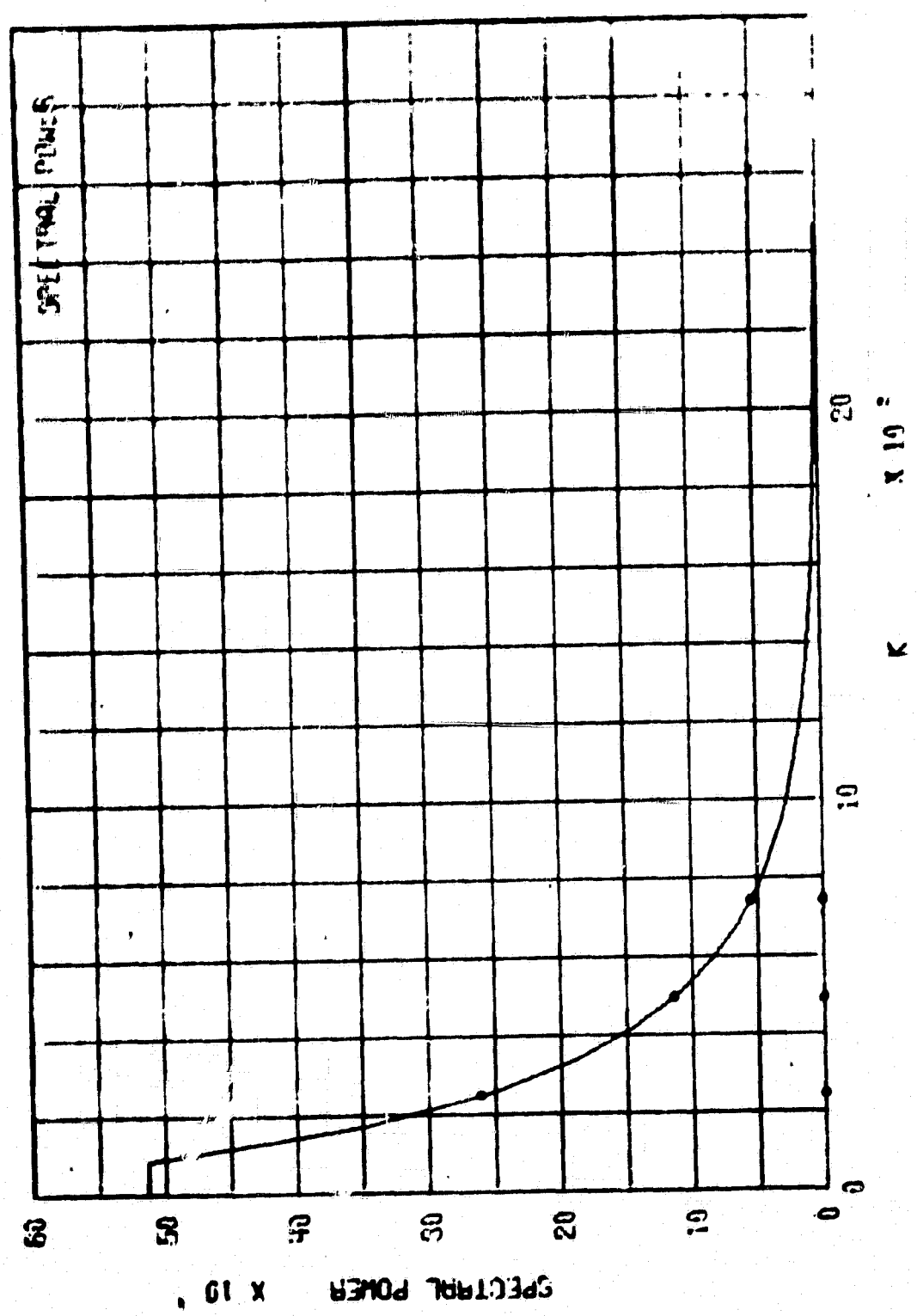

Fig. A-1 Computed Single Pulse Power Spectrum

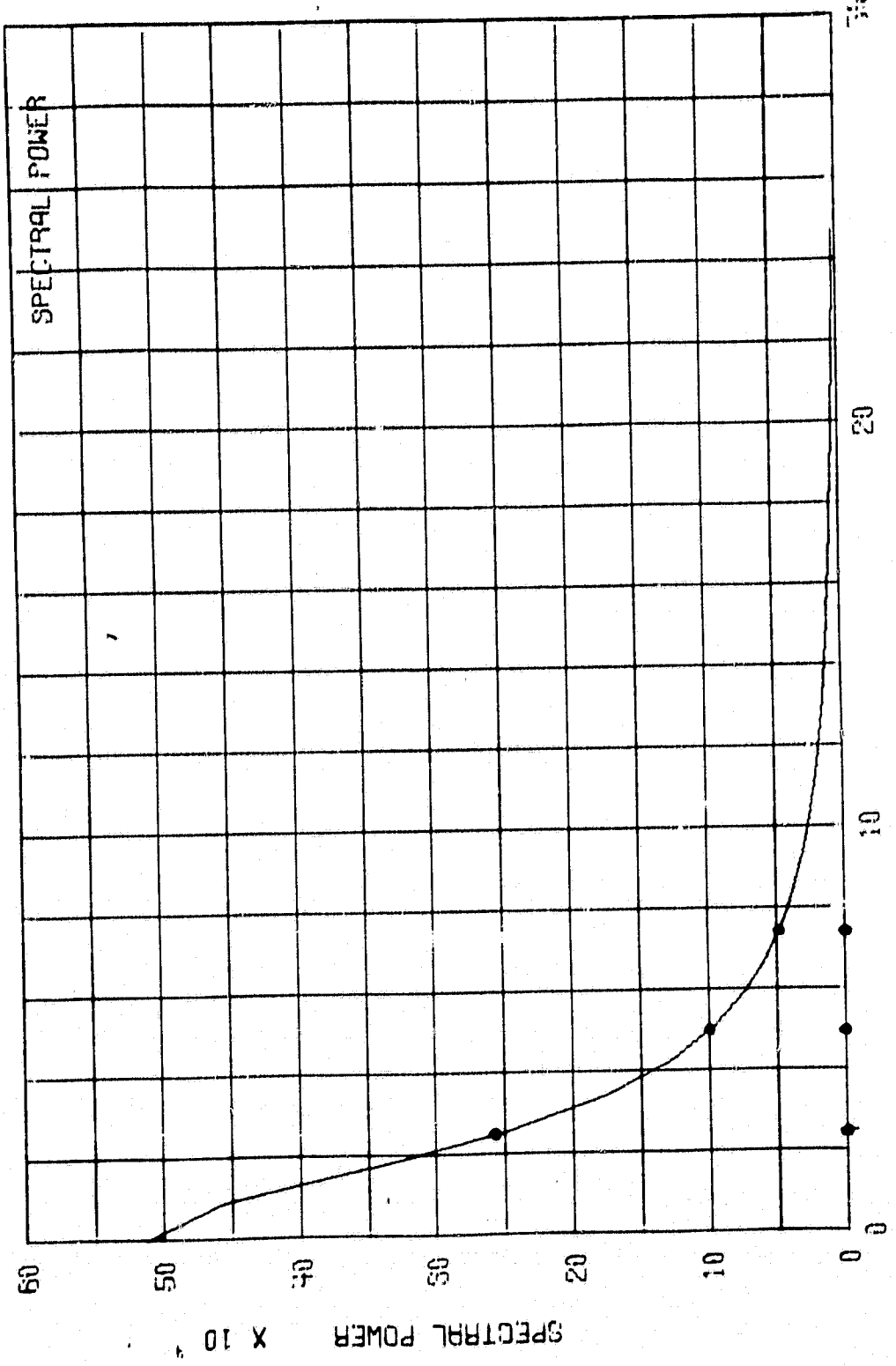

Fig. A-2 Approximated Single Pulse Power Spectrum

APPENDIX B

LEAST SQUARES FIT MINIMIZATION THEOREM

This appendix shows that the vector X computed by (A-7) of the preceding appendix minimizes F(X) given by

$$F(x) = \sum_{k=1}^{n} \delta_k^2 = \Delta^T \Delta \qquad \text{(B-1)}$$

where δ_k are the elements of the n dimensional vector Δ given in (A-4) of the text. For this proof, we show first that F(X) is a convex function. Because it is convex, a vector X that makes F(X) stationary also minimizes F(X)[1]. (If X is chosen so that all partial derivatives of F(X) with respect to the elements of X are zero, then F(X) is stationary for that X.) Finally, we show that the vector X computed by (A-&) of the text makes F(X) stationary.

By definition[2] F is a convex function if Q is positive where

$$Q = (1-S)F(x_1) + S F(x_2) - F\left[(1-S)x_1 + S x_2\right] \qquad \text{(B-2)}$$

X_1 and X_2 are any constant vectors in the domain of F, and S is any real number such that

$$0 < S < 1$$

From (B-1) and (A-4)

$$F(x) = (Ax-d)^T (Ax-d)$$

$$F(x) = x^T A^T A x - 2d^T A x - d^T d \qquad \text{(B-3)}$$

1 J. Abadie, "Nonlinear Programming", North-Holland Publishing Company, Amsterdam, John Wiley & Sons, Inc., New York, p. 104.

2 Op. Cit, p. 99.

where the superscript T indicates the transpose of the matrix or vector. From (B-2) and (B-3)

$$Q = (1-s)\, x_1^T A^T A\, x_1^T + s\, x_2^T A^T A\, x_2^T - \left[(1-s)^2 x_1^T A^T A\, x_1 + s(1-s) x_1^T A^T A\, x_2 + s(1-s) x_2^T A^T A\, x_1 + s^2 x_2^T A^T A\, x_2\right]$$

$$Q = s(1-s)(x_1 - x_2)^T A^T A\, (x_1 - x_2)$$

$$Q = s(1-s)\left[A(x_1 - x_2)\right]^T \left[A(x_1 - x_2)\right] \qquad \text{(B-4)}$$

Since the product of any vector and its transpose must be positive, we can see from (B-4) that Q is positive, with the result that F is a convex function, Let

$$M = A^T A \qquad \text{(B-5)}$$

then from (B-3)

$$F(x) = \sum_{i=1}^{n}\sum_{j=1}^{n} x_i m_{ij} x_j - 2\sum_{i=1}^{n}\sum_{j=1}^{n} d_i a_{ij} x_j - \sum_{i=1}^{n} d_i^2 \qquad \text{(B-6)}$$

where X_i and d_i are elements of the vectors X and d and m_{ij} and a_{ij} are elements of the matrices M and A. From (B-5) we see that M is symmetric, so that

$$m_{ij} = m_{ji} \qquad 1 \le i \le n \qquad 1 \le j \le n \qquad \text{(B-7)}$$

From (B-6) and (B-7)

$$\frac{\partial F(X)}{\partial x_i} = 2\sum_{j=1}^{n} m_{ij} x_j - 2\sum_{j=1}^{n} d_j a_{ji} \qquad 1 \le i \le n$$

and at the stationary point, where these derivatives are all equal to zero,

$$\sum_{j=1}^{n} m_{ij} x_j = \sum_{j=1}^{n} d_j a_{ji} \qquad 1 \le i \le n. \qquad \text{(B-8)}$$

The system of linear equations (B-8) is given in matrix-vector form as

$$M X = A^T d$$

which combines with (B-5) to yield

$$A^T A X = A^T d \quad .$$

PRECEDING PAGE BLANK NOT FILMED.

APPENDIX C

DESIGN OF NOISE WHITENING FILTER

The amplitude response of the whitening filter is given by the following equation:

$$|G(\omega)|^2 = \frac{1}{1 + \frac{1}{N_0 \Delta}|H(\omega)|^2}$$

$H(\omega)$ (= Transform of transition)

is being approximated by:

$$|H(\omega)|^2 = \frac{|H(0)|^2}{1 + b\omega^2 + c\omega^4}$$

leading to

$$|G(\omega)|^2 = \frac{1}{1 + K\frac{1}{1 + b\omega^2 + c\omega^4}} = \frac{1 + b\omega^2 + c\omega^4}{(1+K) + b\omega^2 + c\omega^4}$$

This rational form must be factorizable into $G(\omega) \cdot G(\omega)^*$, $G(\omega)$ and $G(\omega^*)$ being rational forms with real coefficients. This leads to the following possible zeros and poles in the S-plane:

$$\text{zeros:} \quad \pm \sqrt{\left(\frac{b}{2c}\right) \pm \sqrt{\left(\frac{b}{2c}\right)^2 - \frac{1}{c}}} \qquad \text{(C-1)}$$

$$\text{poles:} \quad - \sqrt{\left(\frac{b}{2c}\right) \pm \sqrt{\left(\frac{b}{2c}\right)^2 - \frac{T}{c}}} \qquad T = 1 + C \qquad \text{(C-2)}$$

For a realizable filter the poles are confined to the left half of the S-plane. Possible zero combination:

a) Complex zeros:

$$z_{1,2} = -\sqrt{\left(\frac{b}{2c}\right) \pm \sqrt{\left(\frac{b}{2c}\right)^2 - \frac{1}{c}}}$$

$$z'_{1,2} = +\sqrt{\left(\frac{b}{2c}\right) \pm \sqrt{\left(\frac{b}{2c}\right)^2 - \frac{1}{c}}} \qquad \text{(C-3)}$$

(The first choice corresponds to a minimum phase filter)

b) Additional possibilities for real zeros:

$$z''_{1,2} = -\sqrt{\left(\frac{b}{2c}\right) - \sqrt{\left(\frac{b}{2c}\right)^2 - \frac{1}{c}}} \quad \text{and} \quad +\sqrt{\left(\frac{b}{2c}\right) + \sqrt{\left(\frac{b}{2c}\right)^2 - \frac{1}{c}}}$$

$$z'''_{1,2} = +\sqrt{\left(\frac{b}{2c}\right) - \sqrt{\left(\frac{b}{2c}\right)^2 - \frac{1}{c}}} \quad \text{and} \quad \sqrt{\left(\frac{b}{2c}\right) + \sqrt{\left(\frac{b}{2c}\right)^2 - \frac{1}{c}}} \qquad \text{(C-4)}$$

It is easily verified that for each choice of zeros

$$z_1^2 + z_2^2 = b_1^2 + b_2^2 \qquad \text{(C-5)}$$

This implies a restriction on the pole-zero distribution of

$$G(s) = \frac{(s-z_1)(s-z_2)}{(s-p_1)(s-p_2)}$$

G(s) can be written as

$$G(s) = \frac{s^2 + \alpha s + \beta}{s^2 + A s + B}$$

with $A = -(p_1 + p_2)$ $\quad \alpha = -(z_1 + z_2)$

$B = p_1 \cdot p_2$ $\quad \beta = z_1 \cdot z_2$

where for complex zeros two and for real zeros four choices are possible for z_1 and z_2.

We now show that the above transfer function is always realizable as a "constant R" lattice network:

(For normalized components ($R_o = 1$)

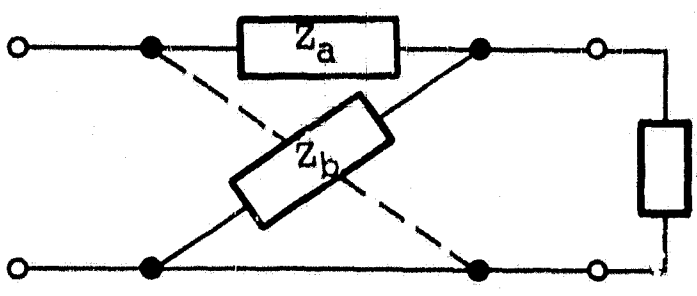

$$Z_a(s) = \frac{1-G(s)}{1+G(s)}$$

$$Z_b(s) = \frac{1}{Z_a(s)}$$

We find for $z_a(s)$ (in normalized components)[1]

$$Z_a(s) = \frac{Ks + M}{s^2 + Ns + 1} \quad \text{with}$$

$$K = \frac{A-\alpha}{2\omega}, \quad M = \frac{B-\beta}{2\omega^2}, \quad N = \frac{A+\alpha}{2\omega}, \quad \omega = \sqrt{\frac{B+\beta}{2}}$$

From their definition it follows that a and b are always positive.

We now show that $A > |\alpha|$. It is sufficient to show that $A^2 > |\alpha|^2$, which means

$$(b_1 + b_2)^2 > (z_1 + z_2)^2$$

Using (C-5) gives

$$p_1 p_2 > z_1 z_2$$

Since $p_1 p_2$ is always positive this holds for negative $(z_1 z_2)$ products. For positive products (cases $z_{1,2}$ and $z'_{1,2}$)

---

1 W. H. Chen, "Linear Network Design and Synthesis," p. 378.

$$z_1 z_2 = \pm\sqrt{\frac{1}{C}}$$

The pole-product is determined by

$$p_1 p_2 = \pm\sqrt{\frac{T}{C}}$$

Since $T = 1 + K > 0$ the above inequality is always satisfied. Similarly, it follows that $B > |\beta|$.

We have now proven that K, M, N and W are always positive real values and hence can represent actual circuit elements. It is readily verified that the following network gives $z_a(s)$:

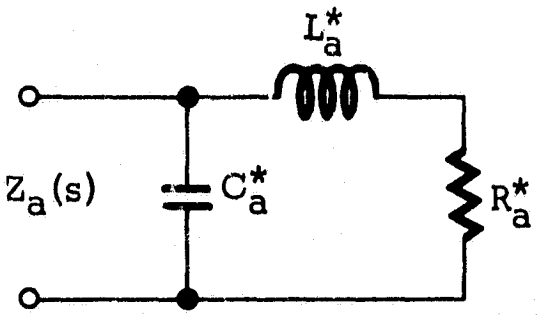

$$L_a^* = K$$
$$R_a^* = M$$
$$C_a^* = N/M$$

The impedance z_b is represented by the dual network[1] (since $z_a \cdot z_b = 1$):

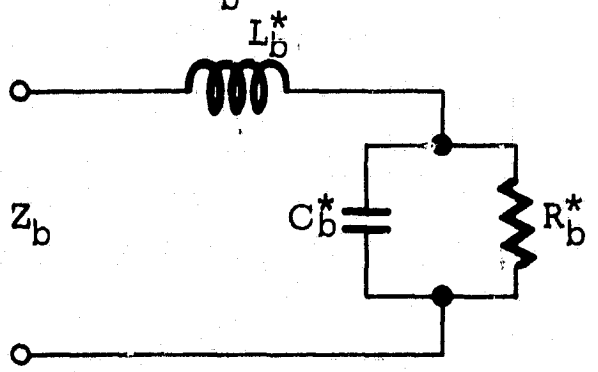

$$L_b^* = C_a^*$$
$$C_b^* = L_a^*$$
$$R_a^* \cdot R_b^* = 1$$

The real element values are given by the normalized values, the termination resistance and the resonant frequency ω :[1]

$$R = R^* \cdot R_0 \qquad C = C^* \cdot \frac{1}{\omega R_0}$$

$$L = L^* \cdot \frac{R_0}{\omega}$$

1 W. H. Chen, "Linear Network Design and Synthesis," p. 378.